6-2009

Physical effects of the respiratory syncytial virus on human cells.

Adam Pfendt 1985-
University of Louisville

PHYSICAL EFFECTS OF THE RESPIRATORY SYNCYTIAL VIRUS ON HUMAN CELLS

By

Adam Pfendt
B.S., University of Louisville, 2008

A Thesis
Submitted to the Faculty of the
University of Louisville
J. B. Speed School of Engineering
as Partial Fulfillment of the Requirements
for the Professional Degree

MASTER OF ENGINEERING

Department of Chemical Engineering

June 2009

PHYSICAL EFFECTS OF THE RESPIRATORY SYNCYTIAL VIRUS
ON HUMAN CELLS

Submitted by:_____
Adam Palmer Pfendt

A Thesis Approved On

JUNE 29, 2009
(Date)

by the Following Reading and Examination Committee:

_____
Dr. Gerold Willing, Thesis Director

_____
Dr. Eric Berson

_____
Dr. Francis Zamborini

ACKNOWLEDGMENTS

The author would like to thank Dr. Willing for all his guidance and mentoring over the years and for providing the opportunity to work as part of his research team, Dr. Shree Singh for funding and support of the project, Seyhan Broyoglu for preparation of the samples used, Dr. Lijian Chen for statistics and analysis support, James Lee and Sudhira Pasupuleti for their friendship and instruction, and Dr. Eric Berson and Dr. Francis Zamborini for their willingness to serve on the thesis review committee.

ABSTRACT

Respiratory syncytial virus is the leading cause of lower respiratory tract infection in infants and currently lacks an effective vaccine or treatment beyond symptom relief. The atomic force microscope is particularly well suited for imaging biological samples including DNA, proteins, cells, and viral activity. Analyzing fixed HEp-2 cells with the AFM after infection and incubation with RSV for periods up to 24 hrs reveals several physical changes that may lead to a better understanding of the viral effects on living cells. Comparing cells fixed with methanol or glutaraldehyde and osmium tetroxide suggests substantial volume losses in the cells regardless of the fixatives used. Suggested mechanisms for the volume decrease include a combination of the creation of an osmotic pressure gradient within the cell and overall cellular collapse. Elastic modulus calculations were performed on the fixed cells at each duration of infection and analyzed for correlations to other physical properties. Hydrophobic interaction forces were also measured and analyzed in order to characterize chemical changes to the cell membrane. It was found that the elastic modulus did not decrease throughout the entire infection for up to 24 hours, but the hydrophobic expression on the cell surface steadily decreased over this same period. This decrease is attributed to the rapid removal and repair of the cell membrane by the RSV virions during exocytosis. Based on this study on methanol fixed cells, it was confirmed that RSV infection does not appear to modify the actin cytoskeleton of human cells.

TABLE OF CONTENTS

NOMENCLATURE

d	Cantilever Deflection
E	Modulus of Elasticity
E^*	Indenter-sample Reduced Modulus of Elasticity
F	Cantilever Loading Force
h_c	Tip Contact Depth
k	Cantilever Spring Constant
M	A Known Mass
m_b	Mass of Beam
m^*	Cantilever Effective Mass
r_c	Indenter-sample Contact Radius
S	Indenter-sample Contact Stiffness
z	Piezotranslator Displacement Distance
α	Cone Half-opening Angle
δ	Tip Indentation Distance
ν	Poisson Ratio
ν_0	Unloaded Resonant Frequency
ν_1	Loaded Resonant Frequency

LIST OF TABLES

LIST OF FIGURES

I. INTRODUCTION

A. Atomic Force Microscopy Background

1. History

Atomic force microscopes first became widespread after their development by Binnig *et al.* in large part because of their comparatively inexpensive production cost and portability. Atomic force microscopy differs from other techniques commonly applied for imaging nanoscale structures and materials in the basic principle of acquiring images based on the interactive forces between a probe and a sample. This independence from electron transmission, scanning, or scanning-tunneling allows for imaging of samples without regard to their conductivity or requiring metallic deposition which limits the variety of potential applications. By measuring the interaction forces between the probe tip and sample, atomic force microscopes (AFMs) have achieved atomic scale resolutions (Binnig et al. 1987) and due to the principles of their imaging are often used in a variety of applications: mechanical response characteristics of samples, surface friction measurements, quantifying magnetization characteristics, depositing and mapping charge density, and characterization of biological samples (Radmacher et al. 1992; Weisenhorn et al. 1989). Imaging may occur under ultra-high vacuum (UHV), cryogenic temperatures, ambient conditions, air, water, or physiological buffer solutions with relative ease allowing for analysis of a sample in conditions similar to those where it might be used, created, or live (Radmacher et al. 1992).

2. Atomic Force Microscopy

In order to generate an image, a cantilever spring suspends a nanoscale tip over a sample at distances of up to several nanometers and measures the attractive or repulsive forces between the tip and surface by the deflection of the cantilever spring (Binnig, Quate, and Gerber 1986; Weisenhorn et al. 1989). The tip, which can be fabricated from a variety of materials depending on the properties desired, is grown and cut on a cantilever during manufacturing and its position relative to the sample is controlled by the electronics of the microscope. The cantilever connects to the AFM by means of a piezoelectric translator which controls the tip position by charge-induced displacement of the piezoelectric materials in three dimensions. The piezoelectric materials, often lead-zirconium titanates, respond to electrical impulses through physical deflection along their lengths. Older AFM technology often employed the use of a single device for three dimensional translation called a piezotube. While current instruments may employ several separate piezoelectric actuators for the x, y, and z dimensions, they operate on the same basic principles as the original piezotubes. The division of the tube into four separate piezoelectric quadrants allows for two dimensional movement of the AFM probe by application of charges to alternate quadrants of

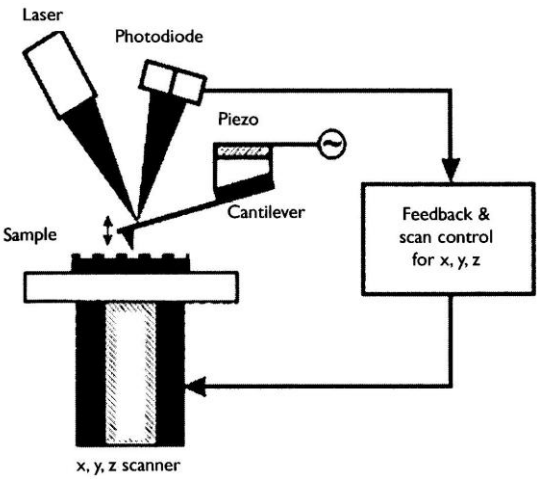

FIGURE 1 – AFM Diagram

(Wilson 2002)

the piezoelectric translator. Elongation or retraction of the tube is achieved through the simultaneous electrical stimulation of all the material present. Technology developed within the past twenty years allows for accurate piezoelectric control of cantilever position to fractions of atomic diameters (Radmacher et al. 1992).

Tip deflection is measured by application of an optical lever. A laser reflects a synchronized beam of light off the cantilever (often gold plated to increase reflectivity for SiN_4 cantilevers and Al plated for Si cantilevers (Wilson 2002)) and onto a photodiode (Figure 1). This photodiode, divided into four quadrants with the laser centered in the middle while at rest, is capable of detecting deflection in the reflected laser as small as 1 nm (Wilson 2002). This high sensitivity is necessary in order to accurately measure the vibrations in the cantilever. The limiting factor on image resolution thusly lies with the tip geometry.

AFM cantilever tips interact with the surface of the sample through forces of attraction and repulsion that can be modified depending on the materials of construction, tip modifications, distance of separation, and tip dimensions. Achievable resolution of the AFM is a function of several aspects of operation with one of the

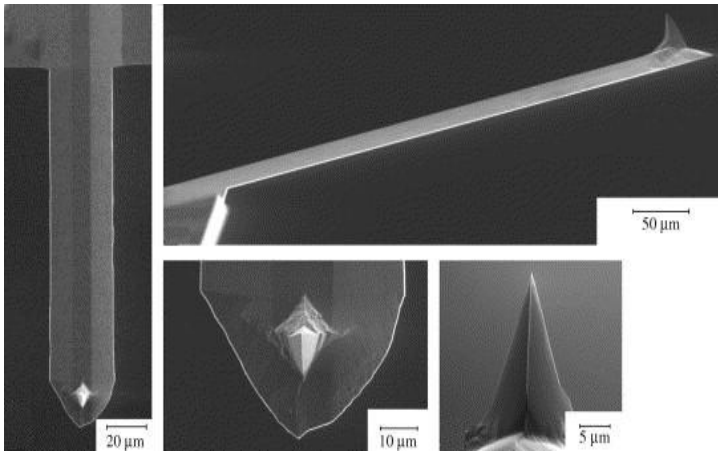

FIGURE 2 – SEM Image of AFM Tips

(Kopycinska-Muller, Geiss, and Hurley 2006)

most important being tip diameter (Radmacher et al. 1992). Commercially available tips range anywhere from 500 nm in length and 100 nm in diameter down to less than 5 nm in diameter (Wilson 2002), and are fabricated in a range of geometries: cylindrical, spherical, pyramidal (Figure 2), or other revolutions of paraboloids. Tips with significantly smaller diameters can be individually fabricated and are often dubbed "super-tips." These structures provide better imaging capability than most commercially constructed tips (Radmacher et al. 1992). The useful life of a probe tip depends on the number of images for which it was used, as well as the nature of the samples. Hard samples may deform a tip more readily than softer samples and thusly reduce the image quality, but soft samples often deposit material on the tip itself over time, requiring cleaning of the tip. Resolution achievable for hard samples imaged with the AFM depends primarily on the surface features and tip geometry. Tips with high aspect ratios or smaller radii will return an image that is more accurate in the X and Y dimensions than a larger tip. Forces affecting the sides of a larger tip will interact with raised surface features well in advance of the sharpest extremity, causing significant distortion on size measurements taken in the X and Y planes. The most accurate dimensioning for atomic force microscopes occurs along the Z axis, and many instruments include separate Z-detectors for greater accuracy. Sharper tips also exert less total force on the sample itself since putting fewer molecules in close proximity with the surface results in less attraction, repulsion, and friction. Minimizing these forces becomes especially important when applied to the imaging of deformable samples such as live cells, DNA molecules, and proteins. Soft samples add an additional consideration in that the sample itself may be deformed or damaged by contact with the probe tip, so the viscoelastic properties of

the sample significantly impact the achievable resolution of the instrument (Lyubchenko et al. 1993; Radmacher et al. 1992).

AFM scanning typically occurs in one of three modes of operation: contact mode, non-contact mode, and intermittent contact mode. In the contact mode of operation (C-AFM), the tip remains in physical contact with the sample during operation and the force on the cantilever is kept approximately constant by means of a feedback loop controlling the piezoelectric translator. Non-contact (NC-AFM) mode operation requires that a certain distance is maintained so that the sample and tip never come into contact if done correctly. By vibrating the cantilever at its resonant frequency and measuring the variations in amplitude and phase of its oscillations, surface characteristics can be discerned. Intermittent contact mode (often called "tapping" mode) combines aspects of the other two modes of operation. The cantilever is again vibrated at a resonant frequency, but the tip comes into contact with the sample surface at the lowest extreme of each oscillation (Matsumoto et al. 1999). Higher resolutions and clarity are observed through contact operation, but at the expense of subjecting the tip to a maximum amount of surface forces and interactions. Intermittent contact mode minimizes these forces by decreasing the amount of time the tip is in contact with the sample. IC-AFM is particularly well suited for imaging of live cells since at high frequencies, the membranes no longer deform due to the viscoelastic properties of the cell (Putman et al. 1994). Membrane deformation from contact mode operation significantly limits the achievable resolutions on AFM imaging of live cells.

Atomic force microscopy has been used for probing mechanical properties of cells and membranes (Radmacher 2002), high-resolution imaging (Jena 2002; Putman et

al. 1994), elasticity and adhesion measurements (Sirghi et al. 2008), and whole single-cell mechanics (Lulevich et al. 2006). Nanoneedles may be fabricated onto cantilevers or AFM tips to allow for micro-scale cell surgeries (Obataya et al. 2005) or injection of proteins, drugs or genetic materials into individual cells (King 2004). Many microbes have been imaged through AFM techniques under natural conditions, a method unique to AFM operation (Dufrene 2008).

3. AFM Imaging of Live and Fixed Cells

Atomic force microscopy provides a relatively unobtrusive method for direct imaging of biological samples that would otherwise be destroyed from vacuum dependent or high energy imaging techniques. Observation of cell movement, growth, and division as well as drug interactions over time have become possible in recent years. Due to the soft nature of living cellular components and membranes, there is potentially a significant amount of deformation in the sample during imaging. This deformation will limit the achievable resolution and make structures appear blurred as they move in response to the contact with the cantilever tip. The contact forces may be so large as to tear the membrane with the tip, however, in living cells the tear is often repaired soon after being damaged (Henderson, Haydon, and Sakaguchi 1992).

Imaging live cells often proves difficult, as they must be kept in enriched solutions at specific conditions in order to keep them alive for as long as possible during imaging. The cells must also be immobilized to a surface in order to minimize their movement when influenced by the forces of tip interaction. Despite the care taken, the lifespan of the cells under these conditions is often only a few hours and the ability to reuse specific samples is limited. Cellular fixation is a common solution to several of the

problems associated with imaging of living samples. Many different chemical compounds, often diluted, are employed to kill and preserve cells with minimal disruption of their living characteristics. Glutaraldehyde, formaldehyde, methanol, methanol/acetone, paraformaldehyde, ethanol/acetic acid, and other fixative mixtures are often employed (Moloney, McDonnell, and O'Shea 2004b). Of note to this work is the use of diluted methanol or glutaraldehyde followed by osmium tetroxide solutions to fix cells. Glutaraldehyde kills the cells and cross-links the proteins within the cell, serving as the primary fixative. Osmium tetroxide works as an oxidative catalyst to cross-link cellular lipids, cross-link proteins such as tryptophan and histidine, and stabilize cellular proteins of the protoplasm (Bourne, Danielli, and Jeon 1969). Application of glutaraldehyde followed by osmium tetroxide as fixatives effectively freezes the cell cytoplasm, lipids, and organelles and increases the observable resolution of the cells for atomic force microscopy (Braet et al. 1998; Radmacher et al. 1992). Fixation via methanol causes proteins to precipitate onto the cellular structure and dehydrates the cell. Imaging of fixed cells often results in distortion or the presence of artifacts, but it allows the repeated use of samples, the ability to store samples for prolonged periods, and increases the resolution of imaging as fixed cells are more rigid than living cells.

4. Non-Imaging Applications

Atomic force microscopy, being based on physical interactions, allows for a unique set of applications that are unavailable for other types of nano-scale imaging devices. AFM tip modifications alter the function of the instrument from depending on physical surface interaction forces to being extremely sensitive to more specific interactions. Applying an electric bias to the tip allows for mapping of surface charge

density with high spatial resolution (Heinz and Hoh 1999). Through measurement of torsion or horizontal cantilever bending, localized friction measurements may be obtained (Erlandsson et al. 1988; Mate et al. 1988; Radmacher et al. 1992). The tip itself may also be physically modified by attaching various interactive molecules such as hydrophobic or hydrophilic compounds, DNA nucleotides, proteins, lipids, reactive species, or functional groups (Butt, Cappella, and Kappl 2005). Typically, imaging through attachment of molecules that alter the primary interactive forces observed by the AFM has been dubbed chemical force microscopy (Dague et al. 2007). CFM allows for mapping of individual molecules across a surface, concentration measurements, and quantitative analysis of chemical interactions.

5. Force Spectroscopy AFM

Instead of moving the tip across or above a particular surface, if the cantilever is held laterally stationary and lowered past the point of first contact, indentations can be made in the sample. To continue pushing the tip into the sample requires an increased voltage applied to the piezo actuator. When the applied voltage is mapped against the vertical position of the cantilever tip, nanoscale mechanical properties of the sample may be studied. Of particular interest in this experiment is the determination of the Young modulus or modulus of elasticity. This quantity is defined by the ratio of stress to strain. When applied to a planar elastic material such as cell membranes, the

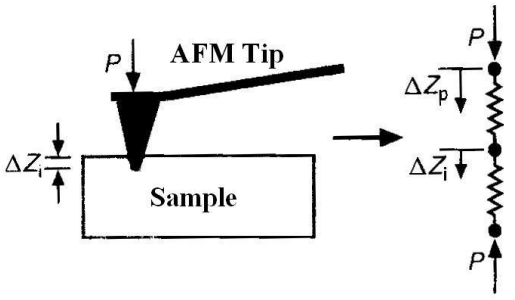

FIGURE 3 – Two Spring Model

(Vanlandingham et al. 1997)

elasticity is calculated as a function of pressure and the vertical distance the tip travels into the membrane. Since both the membrane and the cantilever itself are flexible, the system is appropriately modeled by two springs in series (Figure 3). Some additional calculations and measurements must be made in order to accurately model this system in order to provide for the impact of the cantilever flexion on the elasticity analysis. Nominal values of the spring constant and resonant frequency of the cantilever are given by the manufacturer, but for calculation of material mechanical properties, these values must be determined as accurately as possible (Cleveland et al. 1993).

The elastic modulus of cells is a limiting factor for C-AFM imaging resolution (Braet et al. 1998). Live cells tend to have elastic moduli between 1kPa and 100kPa (Rotsch, Jacobson, and Radmacher 1998) but after fixation by glutaraldehyde, significant increases in elastic modulus and thusly image resolution have been identified (Braet et al. 1998). Various researchers frequently employ several different models to calculate elastic moduli from force-distance curves generated by AFM including the Hertz model (Hertz and Reine 1882), Sneddon theory (Sneddon 1965), or other derivations based on these models to decouple various forces involved such as adhesion (Sirghi et al. 2008).

B. Respiratory Syncytial Virus Background

1. RSV Infection Statistics

Respiratory syncytial virus (RSV) predominately infects the upper respiratory tracts (cold-like symptoms) of infants and the elderly, however severe lower respiratory tract infections such as bronchiolitis and pneumonia do occur. For infants under one year of age, RSV is the most common cause of bronchiolitis, an inflammation of the bronchioles or smallest airways in the lungs (Thompson et al. 2003). RSV infections can

lead to cardiac and pulmonary complications, asthma, and mortality in infants and the elderly (Thompson et al. 2003). Nearly all infants have an RSV infection by the age of two and 25-40% will exhibit symptoms of lower respiratory tract infections (Center for Disease Control 2008). More than 80,000 infants are hospitalized due to RSV infections and about 1,600 die each year in the United States (Center for Disease Control 2004). It is estimated that 64 million RSV infections occur every year resulting in 160,000 deaths across the globe (World Health Organization 2005). Typical recovery of most cases occurs within one to two weeks without requiring treatment, but up to 2% of infants infected for the first time require hospitalization (Center for Disease Control 2008). Rapid antigen detection methods are insensitive to adults, leading to rare diagnosis of RSV infections in this demographic (Thompson et al. 2003). RSV predominantly afflicts infants in terms of number of infections, however more than 78% of all RSV-associated underlying respiratory and circulatory deaths occurred in those above 65 years of age (Thompson et al. 2003).

2. RSV Symptoms, Transmission, and Treatment

Initial symptoms such as rhinorrhea (nasal mucous discharge) or a decrease in appetite typically develop four to six days after exposure to RSV, followed by coughing, sneezing, fever, and wheezing (Center for Disease Control 2008). In infants and young children, difficulty in breathing often causes a bluish tint in the skin of the lips or fingernails resulting from decreased oxygenation of the blood (American Lung Association 2004).

RSV spreads through interaction with contagious individuals, mucous and saliva emitted by sneezing or coughing, and contact with contaminated surfaces. RSV is able to

survive for many hours on harder surfaces such as desks or tables, but hands and tissues render this virus harmless after shorter durations. Sneezing or coughing will emit droplets of saliva that are able to transmit the virus through the air and are infectious if contacting the epithelia of the eye, nose, or mouth. Outbreaks of RSV typically occur during the coldest months of the year and can spread though families and communities rapidly, lasting between four and six months. (Center for Disease Control 2008) Often, RSV infections are mistakenly diagnosed as influenza, and some deaths have been mistakenly attributed to complications of influenza as well (Nicholson 1996).

In most cases of mild infection in children, recovery occurs without any treatment besides that used to alleviate the symptoms. More severe cases require respiratory aid such as oxygen, intubation, or mechanical ventilation until the virus is suppressed by the immune system. In order to treat patients with deficient immune systems, a combination of medicines are administered: immune globulin intravenous (IGIV) with high titers of neutralizing RSV antibody (RSV-IGIV) and ribavirin (Nath and Revankar 2005).

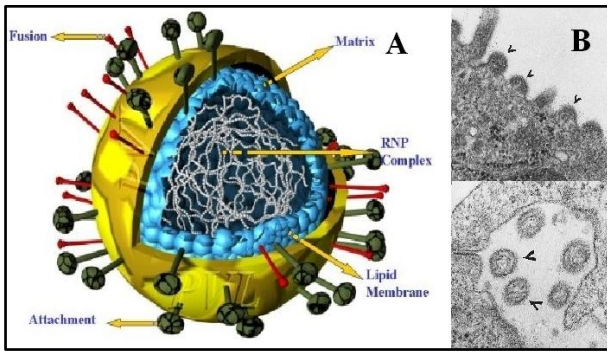

FIGURE 4 – RSV Structure

(A) An artisitic depiction of the RSV general structure shows several of the predominately expressed proteins in the viral structure (Easton 2000). (B) Electron microscopy portrays RSV budding from the apical surface of Vero C1008 cells (Roberts, Compans, and Wertz 1995).

3. Structure, Components, and Functions

The human respiratory syncytial virus is categorized as a single-strand, negative-sense RNA virus of the family *Paramyxoviridae*, subfamily *Pneumovirinae*, and

Pneumovirus genus. Negative-sense RNA must first be transcribed into its positive-sense RNA complement by an RNA polymerase, sometimes carried inside the virion. The RNA strand consists of 15,222 nucleotides (World Health Organization 2005) that are encapsulated by the nucleocapsid (N) protein. The N protein also interacts with the viral RNA and RNA polymerase molecules during transcription. The matrix (M) protein is found between the nucleocapsid and the virion envelope that is formed from the plasma membrane of the host cell during exocytosis. The lipid membrane exhibits fusion (F) proteins, attachment (G) proteins, and small hydrophobic (SH) proteins. Three additional proteins encoded by the RSV genetic material are thought to regulate RNA synthesis or to suppress the immune response of the host cell. Figure 4 shows an artistic depiction of the RSV virus (A) as well as electron microscopy of an infected Vero C1008 cell (B). The G protein, responsible for attachment of the virus to a host cell, varies between the two different strains of RSV. The F protein, responsible for joining the viral envelope with the target cell membrane, remains constant between strains and is subsequently the target of vaccine development (World Health Organization 2005). (Collins and Murphy 2001; World Health Organization 2005)

C. Experimental Design and Theory

1. Experimental Objectives

Human epithelial cells are to be analyzed using the AFM in order to detect changes resulting from infection by the respiratory syncytial virus. Several properties of the cells will be studied for periods of infection from 0 to 24 hours including visual changes, mechanical properties, and chemical composition of the cell membranes. Visual changes will be detected through analysis of images acquired in by contact mode AFM

operation. Mechanical properties will be studied by calculating the elastic modulus of the cell cytoskeleton at specific points of indentation by the AFM in force-distance spectroscopy operation. The hydrophobic nature of the cell membrane and extracellular matrix will be studied by analysis of the adhesion forces between the cell surface and the AFM tip. All of these properties will be measured after infection by RSV for periods of 0, 0.5, 4, 8, 16, and 24 hours in order to determine if the effects of this virus can be detected in methanol fixed cells via AFM techniques.

2. Basis of Experiment: Cell Volume and Membrane Elasticity

Work done by Lee et al. describes the formation of pores in the cell membrane as an effect from infection with RSV. Holes are suspected to result from the rampant exocytosis of the replicated viruses as they leave the host cell. These large gaps in the lipid bilayer facilitate loss of cytoplasm and a subsequent decrease in cell volume over the progression of the infection. As the virus breaks down proteins and structural materials to make its capsid and other components, the height and clarity of the cell tend to deteriorate over time (Lee 2006). In order to quantitatively estimate the volume changes in the cell, step height measurements were taken after imaging in non-contact mode with the AFM. The step height from the substrate to the cell membrane was measured for cells incubated with the RS virus for increasing periods of time.

The deterioration of the cell cytoskeleton, membrane, and organelles should have another observable effect besides an impact on the cellular volume. It is hypothesized that the elastic modulus of the cell should decrease over the duration of an RSV infection as the membrane becomes more porous and the supporting structure degenerates. By using the AFM to acquire force-distance measurements of fixed cells at various durations

of infection, quantitative measurements of the change in cellular elasticity should be possible. Since the cell membrane may stretch when depressed by an AFM tip without imparting any noticeable resistance (Sirghi et al. 2008), the elastic modulus of a cell most heavily depends on the characteristics of the actin cytoskeleton (Sackmann 1994). The elastic force from the cell membrane is typically neglected in elastic modulus calculations (Seifert and Lipowsky 1995).

3. Cantilever Spring Constant and Resonant Frequency

When using the AFM in contact mode, the set point is an input value of the maximum allowable force between the tip and the sample calculated from the deflection voltage and the cantilever spring constant (Butt et al. 1993). For the purposes of imaging, an order of magnitude approximation is all that is necessary for typical operation (Albrecht et al. 1990). Before probing the cell surface to create force-displacement curves used in elasticity determination, calibration of the AFM must first occur by inputting an accurate measurement of the resonant frequency and spring constant of that particular cantilever (Cleveland et al. 1993). These values are used to internally convert the required voltage to a measure of applied force. Without this calibration, relative changes in elasticity may be detected and compared, but these values would hold no bearing on any measurements utilizing a different cantilever or instrument. Determination of the spring constant and effective mass is possible by measuring the changes in resonant frequency caused by suspending known masses from the cantilever. These calculations are based on equations published by Cleveland et al. (1993). Spring constants of cantilevers can be calculated using beam theory, and for V-shaped

cantilevers, two rectangular beams operating in parallel accurately model the system behavior (Butt et al. 1993).

Determination of the spring constant (k) for a cantilever is achieved by measuring the resonant frequency (v) of the beam after suspending a known mass (M) from the free end as per Eq. (1) below.

$$v = \frac{1}{2\pi}\sqrt{\frac{k}{M+m^*}} \tag{1}$$

The effective mass of a uniform, rectangular cantilever m^* is approximately 0.24 times the mass of the beam m_b. By using this equation with a series of known masses, Cleveland et al. (1993) were able to derive a relationship allowing for the accurate calculation of the spring constant based on the unloaded resonant frequency v_0 and the resonant frequency v_1 obtained with one added mass M_1:

$$k = (2\pi)^2 \frac{M1}{1/{v_1}^2 - 1/{v_0}^2} \tag{2}$$

4. Force-Distance Data Interpretation

After indentation of a cell membrane with a C-AFM tip is achieved, and the characteristic force-displacement curve is generated, the data must be fit to a proven model in order to calculate the sample elasticity. Typical force-displacement curves

consist of several regions: no contact, transition, repulsive, and adhesion as seen in Figure 5.

As the tip approaches the sample but before it begins to interact at the surface, the applied force is independent of tip displacement. This results in the flat, linear no contact portion of the graph. The tip continues to approach the sample surface and enters into a transition region where the capillary and adhesive long range forces of the membrane attract the tip. In this transition region of the approach, the surface-tip interactions cause a variable drop in the amount of force required to lower the tip until the tip reaches the sample surface. Once contact is made, the amount of force required to lower the tip into the sample surface increases linearly with the distance traveled. This is the repulsive

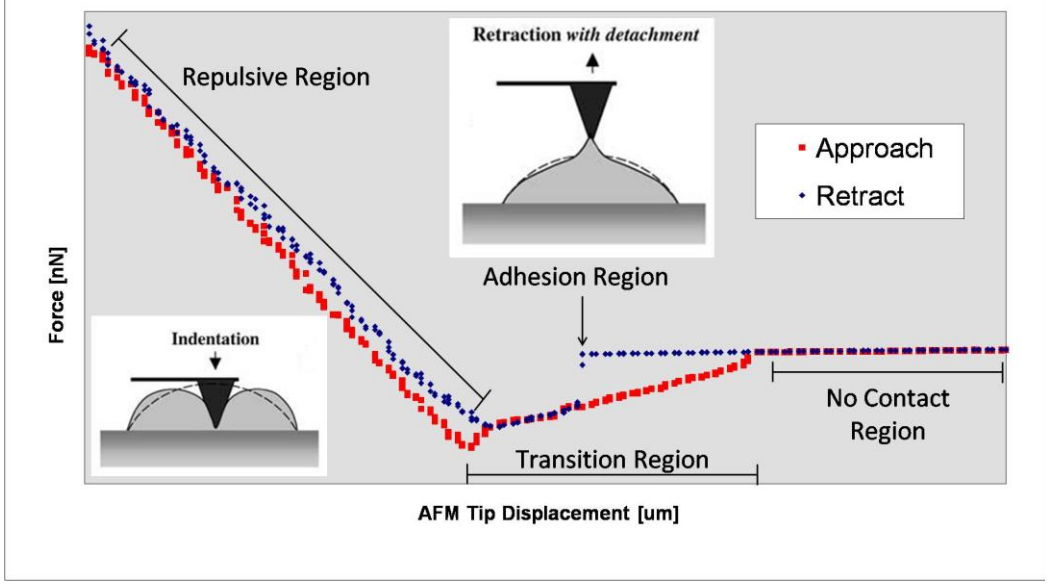

FIGURE 5 – Example F/D Curve

This plot shows the different regions of a typical force-displacement curve. Inset pictures show tip indentation and adhesive forces during retraction (Sen, Subramanian, and Discher 2005). The tip approaches from right to left and retracts in the opposite direction on this graph.

region of indentation, where the sample exerts a force on the tip opposing the movement sustained by the piezoelectric translator. The tip will continue to indent the sample until a maximum, specified force is reached at which point it will reverse direction and begin retracting. In Figure 5, the tip retraction data is represented by the blue dots and should be read from left to right. While the tip is being retracted, the membrane adhesive forces attract the tip causing the membrane to deform in the opposite direction as the tip rises above its resting surface position. When the adhesive forces are no longer able to keep the membrane in contact with the tip, the cell surface will detach from the probe and fall back to its normal resting position. This region of attraction ends with a steep increase in force back to the no contact magnitude. Because surface-indenter adhesion may significantly impact the retraction or unloading portion of the curve, several researchers have used the loading section for determinations of cell elasticity (Radmacher 2002).

Before analysis of this graph to determine the elastic modulus of the cell can be undertaken, another force-distance curve must be generated. Because both the membrane and cantilever behave as springs, the cantilever will flex as the tip begins to indent the cell surface. This flexion of the cantilever is proportional to its spring constant and must be taken into account in order to know the true tip displacement. A force-distance curve must be generated using a stiff sample in order to gauge the cantilever flexion as a function of force. For a stiff sample, the graph will appear much more rigid and linear since the surface will not indent. The displacement will continue to change as detected by the piezotube, however in actuality; the tip will not depress the sample. The linear contact portion of this graph is used to model the cantilever indentation into the cell δ as a function of force. The force data generated by the atomic force microscope is initially

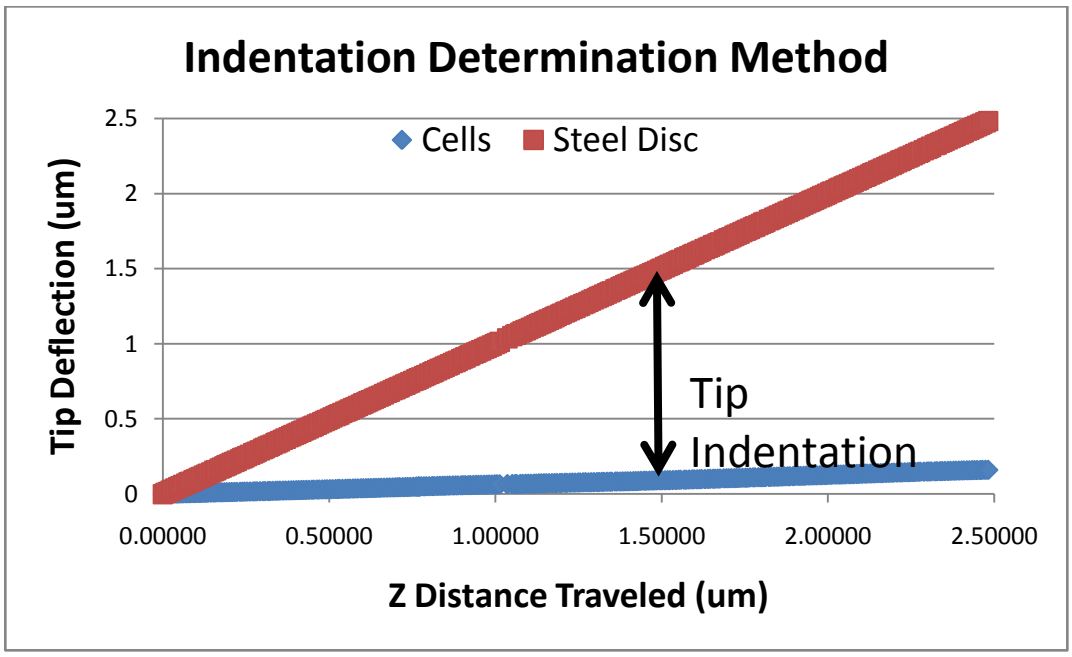

FIGURE 6 – Tip Indentation Graph

plotted against the piezotranslator displacement z when it is recorded by the AFM. Determination of the tip indentation δ into the cell is required for elasticity calculation and is found by subtracting the cantilever deflection d from the piezo displacement by equation (3) and seen graphically in Figure 6 (Sirghi et al. 2008).

$$\delta = z - d \tag{3}$$

The slope of the loading portion of the force-displacement curve in the repulsive region for axis symmetric indenters (such as cylinders, cones, paraboloids, and spheres) is the indenter-sample contact stiffness S given by:

$$S = \frac{dF}{d\delta} = 2 \cdot E^* \cdot r_c \tag{4}$$

where F is the loading force, r_c is the indenter-sample contact radius given by (5), and E^* is the indenter-sample reduced modulus of elasticity (Sneddon 1965).

$$r_c = h_c \cdot \tan\alpha \tag{5}$$

For conical indenters r_c is a function of the contact depth h_c and the tangent of the cone half-opening angle α. Nearly all AFM tips are in fact pyramidal due to their crystalline nature, but the conical assumption is often used for simplification. Assuming that the tip is not deformed by the sample during indentation (valid for hard silicon tips and soft fixed cells), E^* can be approximated by the following formula:

$$E^* = \frac{E}{1-\nu^2} \tag{6}$$

where E is the Young modulus of elasticity, and ν is the Poisson ratio of the sample with a value of 0.5 for incompressible fluids such as cell cytoplasm (Radmacher 2002). The contact depth h_c was assumed to be constant and equal to the indentation δ for simplification. In reality, the contact depth will increase as the tip depresses into the sample up to its maximum indentation. The resulting overall equation for calculation of the cell elastic modulus based on the stated assumptions is given in (7). (Sirghi et al. 2008)

$$E = \frac{\frac{dF}{d\delta}\left(1-\nu^2\right)}{\pi \cdot \delta \cdot \tan\alpha} \tag{7}$$

Original force and piezo-distance data were converted into loading force and indentation data via routines developed in VBA for Microsoft Excel. These routines remove excess data not in areas of interest and also eliminate a common step abnormality found in many of the data sets. The full code for importing the data files into Microsoft Excel, calculations, and elastic modulus calculations may be reviewed in Appendices I, II, and III respectively.

Because the tips being used for indentation were chemically modified by the addition of methyl groups to its surface, it is possible to measure the hydrophobic adhesion forces between the tip and cell membrane. To study the adhesion force between a sample and AFM tip, the retraction curve is analyzed in the adhesion region of FIGURE 5. Strong attractive forces will require a large amount of retraction force in order to separate the cell membrane from the probe tip and create a larger well in a retraction curve. The depth of the well created in the force-distance curves can be measured in order to determine the adhesive force of a sample indentation. In the case of the present study, the well depth is not purely the adhesion interaction between the cell membrane and the AFM tip but is largely a function of the concentration of hydrophobic molecules present on the cell exterior. As the concentration of hydrophobic molecules in the extracellular matrix increases, the hydrophobic adhesion force between the membrane and tip will increase. The analysis of the retraction curve and adhesion well at increasing durations of RSV infection allows for determination of changes to the hydrophobic molecule concentration on the cell membrane. Because the measurement of these forces is heavily dependent on the area of contact between the surface and the probe tip, the interactions between different indentations may only be compared for approximately

equal areas of contact. The adhesion force was measured at the point immediately before membrane-tip separation occurred so as to normalize the adhesion forces measured with approximately equal contact areas. The routines used in the adhesion force analysis are found in Appendix VI.

II. MATERIALS AND METHODS

A. Instrumentation Description

1. Atomic Force Microscope

The primary instrument used in the research discussed herein is the XE-100S Advanced Scanning Probe Microscope manufactured by Park Systems (PSIA) in Suwon, Korea as seen in Figure 7. This instrument provides the capability to analyze samples via true non-contact mode scanning, contact mode operation, tapping mode imaging, lateral force microscopy, force-distance spectroscopy, phase imaging, conductive AFM, scanning tunneling microscopy, magnetic force microscopy, electric force microscopy, scanning capacitance microscopy, scanning thermal microscopy, nanolithography, and nanoindentation. The XE-100 was designed to overcome limitations on achievable resolution for NCAFM imposed by the large separation distance between sample and tip. Consistently maintaining smaller distances of separation is achieved by the designed decoupling of the XY-scanner from the Z-scanner. By using two separate scanners to control the tip-sample interaction, the apparent curvature introduced by conventional piezotube scanners is eliminated, scan speed is typically reduced by an order of magnitude, and the cross-talk

FIGURE 7 –PSIA XE-100 AFM

This model AFM was used for all data acquisition inside of a hermetically sealed enclosure placed on an air table.

and non-linearity issues associated with piezoelectric tube scanning systems are minimized (Park Systems 2008).

The XY-Scanner used to precisely control the raster scanning pattern and sample motion in two dimensions is a body guided flexure scanner with only 1-2nm of out-of-plane motion over a 50 µm scan size. Piezotube scanners typically exhibit 80nm of out-of-plane motion over a similar range. The standard 50µm XY-scanning stage was used for all samples analyzed. (Park Systems 2008)

A high resolution CCD camera mounted directly above the stage provides a 480µm by 360 µm field of view with a standard 780x optical magnification. The maximum achievable resolution using this optical microscope is 1µm. This camera and optical microscope allow an on-axis view of the cantilever and sample for enhanced positioning precision and alignment of the laser. The CCD camera is able to generate an image over a 20mm range with motorized focus control. (Park Systems 2008)

This instrument operates inside of a hermetically sealed acoustic enclosure placed on top of a Herzan TS-150 air table manufactured in Laguna Hills, CA. This isolation system is able to significantly negate the effects of vibrations ranging from 0.7 Hz to 1000 Hz.

2. NC-AFM and C-AFM Cantilevers

The noncontact AFM cantilevers used were manufactured by Applied NanoStructures of Phoenix, AZ. These premounted ACTA-10 probes are received glued to metal holders which can be inserted as-received into the XE-100. The rectangular cantilevers are 125 µm long by 45 µm wide and are 4 µm in thickness. The pyramidal tip having a typical radius of curvature of 6 nm but guaranteed to be less than 10 nm and

height between 12 and 16 μm, has a reported spring constant range of 25-75 N/m with resonant frequency of 200-400 kHz. The tips are manufactured from low resistivity (0.001 – 0.025 ohm/cm) antimony doped single crystal silicon to effectively eliminated danger of tip destruction from electrostatic charging and to increase durability (AppNano 2002). The cantilevers have an aluminum reflex coating on the side opposite the tip to increase the reflectivity for the impinging laser.

C-AFM tips were standard tips manufactured by Veeco Instruments (Camarillo, CA) that were individually calibrated and chemically modified by NovaScan Technologies (Ames, IA). These silicon nitride triangular cantilevers were gold coated in order to increase their reflectivity and have a nominal tip radius of 15 nm with a maximum of 20 nm and a height of 2.5 to 3.5 μm. The spring constants of each tip were measured at NovaScan and were found to be 0.15 N/m. The tips were also chemically modified via addition of methyl groups allowing for the measurement of hydrophobic interaction forces from existing data.

It has been reported that the lateral variation from current manufacturing techniques is less than a micrometer (Albrecht et al. 1990). The greatest variation occurs in the thickness dimension, often ranging from 0.4 to 0.7 μm of the reported value, which necessitates the individual calibration of each cantilever for accurate force-distance spectroscopy (Butt et al. 1993).

3. Software

The XE-100 atomic force microscope is controlled via the XEP data acquisition software version 1.6.4. XEP communicates with the instrument in order to translate the raw data into surface images and meaningful graphs. XEP is able to acquire up to 16

images at a time in forward and reverse scanning directions. It allows for automatic control of tilt, contrast, and curvature while imaging a sample and exports TIFF files to the XEI image analysis software.

XEI version 1.6 is used to process all images gathered from the XE-100 and allows for dimensional analysis, statistics, and image processing. The results may then be exported as a data file or image for other use. Image processing capabilities provided by XEI include Fourier power spectrum editing, low pass filter and deglitch, contrast enhancement, and 1^{st} or 2^{nd} order polynomial fit of surface curvature. Analysis functionality includes profile tracing, line profile, height measurements, power spectrum, histograms, region height profiles, average roughness, volume, grain analysis functions, and others.

The high resolution CCD camera feeds images to the computer via the XEC software version 1.1. This simple video feed allows for identification of potential imaging sites on the micrometer scale by use of the optical microscope before detailed scans are made with nanometer resolution.

B. Methods and Procedures

1. Cell Cultures and RSV Preparation

All cell cultures and procedures were carried out as written by Boyoglu et al. and imaged as received. Human body type-2 epithelial cells (HEp-2) purchased from the American Type Culture collection (ATCC, CCL-23) and derived from HeLa contamination of an epidemoid carcinoma of the larynx were propagated according to standard procedures in Minimal Essential Medium (MEM) with 10% Fetal Bovine Serum

(FBS), 2 mM L-Glutamine, 75 U/ml Penicillin, 100 mg/ml Kanamycin, and 75 mg/ml Streptomycin. (ATCC 2008; Boyoglu et al. 2009)

Human respiratory syncytial virus A long strain purchased from ATCC (VR#26) having a multiplicity of infection (m.o.i.) of four to one was added to HEp-2 cells. Adsorption occurred for one hour at 37°C in a 5% CO_2 humidified atmosphere. MEM, 2% FBS, and 2mM of L-Glutamine were added and RSV infection of the cells was observed for a three day period. The infected cells were harvested and the resulting suspensions were put through two freeze-thaw cycles at -80°C. In order to remove cellular debris, these suspensions were centrifuged at 3,000 x g at 4°C. Viral stock was then stored at -80°C or frozen in liquid nitrogen. Plaque assay done on the viral stock measured a viral titer of 10^6 p.f.u. per ml. (Boyoglu et al. 2009)

2. Cell Infection, Fixation, and Preparation for AFM

Hep-2 cells (Human body Type-2 epithelial cells) were seeded in a 12-well plate at a density of $1.8x10^5$ cells per well in 100 µl of MEM with 10% FBS. The seeded cells were then incubated overnight at 37 $^{\circ}$C under a 5% CO_2 atmosphere. After 24 hours, the medium was removed and the cells were infected with 100 plaque-forming units (pfu) of RSV. Cover slips, 20mm in diameter, were added to the same 12-well tissue culture plates after RSV infection. The RSV infected cells grew until their desired density for AFM imaging was reached. The cover slips were washed with 5 ml of phosphate buffered saline (PBS) at incremental time intervals of 0, 0.5, 1, 2, 4, 8, 16, 24, 36 and 48 hours before being transferred into small petri dishes. The cells plated on cover slips were then treated with 400 µl of pure methanol for 30min to fix the cells. This fixation effectively halts cell growth, replication, and processes by precipitating proteins onto the

cellular architecture. After the fixing process, each cover slip was rinsed with 200 µl of deionized water followed by immersion in 70%, 90%, and 100% ethanol solutions for 5 minutes each to dehydrate and inactivate the cells and RSV. The cover slips were then allowed to air dry in a sterile hood and were stored in a Secador 4.0 desiccator cabinet until being used for AFM analysis. This cabinet controls the relative humidity of the internal atmosphere at less than 20% to help reduce the size of the adsorbed water layer on the cell samples.

3. Non-Contact AFM Imaging

Cover slips removed from the dehumidification cabinet were glued to 12mm steel discs purchased from SPI Supplies with Veeco "stickydot" pressure sensitive adhesive. The disc was then labeled and inserted into the AFM for cover slip imaging. Cover slips are suitably smooth when compared to the size of cellular features, but for imaging of RSV a freshly cleaved mica substrate was used. The nanoscale dimensions of the RSV would have been significantly distorted by cover slip height differences, but when compared to a cell several micrometers tall these variations are negligible. After selecting non-contact mode operation, laser alignment, and tip approach occurred, a suitable area of imaging was determined via use of the optical microscope and CCD camera.

Because step height measurements of the cell membrane were to be recorded, preferred areas for imaging were those where the membrane height could be directly compared to that of the cover slip. Once a suitable area was found, scanning began over a 40µm by 40µm area at a raster frequency of 0.4 Hz. Typical starting set point was approximately -0.205 µm, the drive was set to 30% of the maximum voltage and

occasionally increased to enhance resolution, and the Z servo gain was set at a value of 10.

After initial image acquisition, areas of interest were scanned again using a smaller scan area and lower raster frequency in order to decrease the number and magnitude of glitches present. Images were then analyzed using the XEI software to flatten the surfaces using 1st or 2nd order polynomials in both the X and Y directions to level and remove curvature from the images. Contrasts were enhanced and paired cursors were used to measure differences in height on each image at multiple locations. The distance between substrate and first detectable presence of the cell membrane was measured as in Figure 8. These measurements were repeated as often as possible for a single cell in an image in order to reduce the effects of variation within an individual cell. When multiple cells were present and clear in an image,

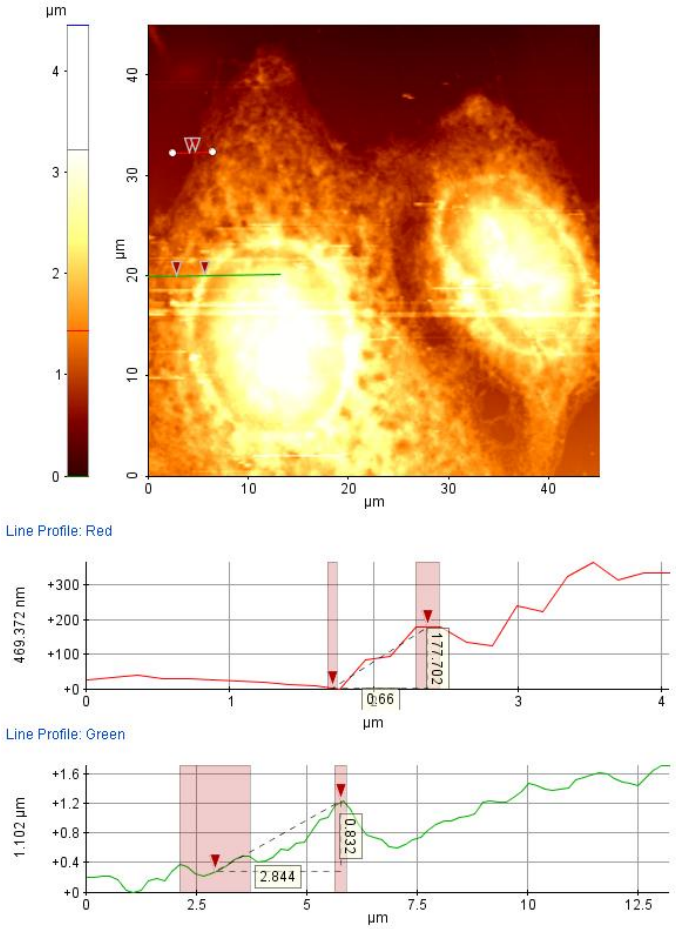

FIGURE 8 – Membrane Step Height Measurements

The lateral measurements between cursors are skewed due to the geometry of the tip leaving the height or Z dimension as the most accurate for acquiring data.

these measurements were repeated for each applicable cell. Otherwise, new areas of the cover slip were scanned and analyzed in a similar fashion. Cells at each time interval were imaged, and the measurements of membrane step heights were recorded for interpretation.

4. C-AFM Imaging and Force-Distance Spectroscopy

Prior to force-distance spectroscopy of fixed cells, promising locations identified via the optical microscope of the AFM were imaged in contact mode. Imaging parameters varied based on the clarity of the first picture obtained. Typical values of scanning parameters are as follows: 45µm by 45µm scan size at 0.8 Hz with a setpoint of 5-10 nN and Z servo gain of 10. Generation of force-distance data typically used the following settings: Z distance travelled from -1.5µm to 1.5µm, approach and retraction speed of 0.5µm/s, and a force limit of 79.1 nN. Piezo displacement speeds of 0.5µm/s or less were utilized in order to minimize the effects of cell viscosity on the cantilever during indentation (Sirghi et al. 2008). Due to cantilever deflection during indentation, the actual tip displacement occurs more slowly than that of the piezotranslator as described in (3). The force-distance data generated was divided into separate categories for analysis depending on the location of the indentation relative to the cell. Membrane data and nuclear data were acquired based on the selected points

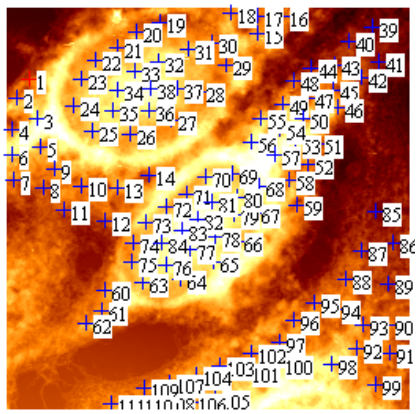

FIGURE 9 – F/D by Relative Cell Location

F/D data gathered at any point within the cell membrane and nucleus were compared, and questionable locations were omitted from consideration.

of indentation as seen in Figure 9, and cover slip data provides a reference sample to study cell membrane hydrophobic forces.

III. RESULTS AND DISCUSSION

A. Image Analysis

1. Qualitative Image Analysis and Fixative Comparison

Previous work describes an observed decrease in the cellular volume as a function of exposure to RSV before fixation (Lee 2006). These results were obtained for cells fixed by a 0.1% glutaraldehyde solution for 30 minutes followed by a treatment of 1% osmium tetroxide for 30 minutes. Measurement of the height of the nuclear envelope compared to an average area of the cell membrane was recorded for a total of 29 different cells fixed after being incubated with RSV for periods of 0, 0.5, 4, 8, 24, and 48 hours. The decrease in height correlating with prolonged duration of infection was not observed in these methanol-fixed cells. The observed trend from previous work by Lee was not strong and occurred over measurements taken on a smaller number of samples. In order for a statistically significant correlation to be observed, many more cells likely require measurements as compared to the dozens that were analyzed. It is important to note that the trend observed by Lee should not be readily discredited, since methanol fixation of cells has been known to produce swelling of the nucleus and organelles distorting any height measurements obtained (Hahm and Anderer 2006).

While it has been shown that methanol fixation promotes swelling of the nucleus and nucleoli, significantly damages cellular structure and organelles, and promotes protein extraction (Hahm and Anderer 2006; Hoetelmans et al. 2001), several characteristics were observed in both the cells fixed by methanol and by osmium tetroxide (imaged by Lee). The osmium tetroxide fixed cell in Figure 10A was part of

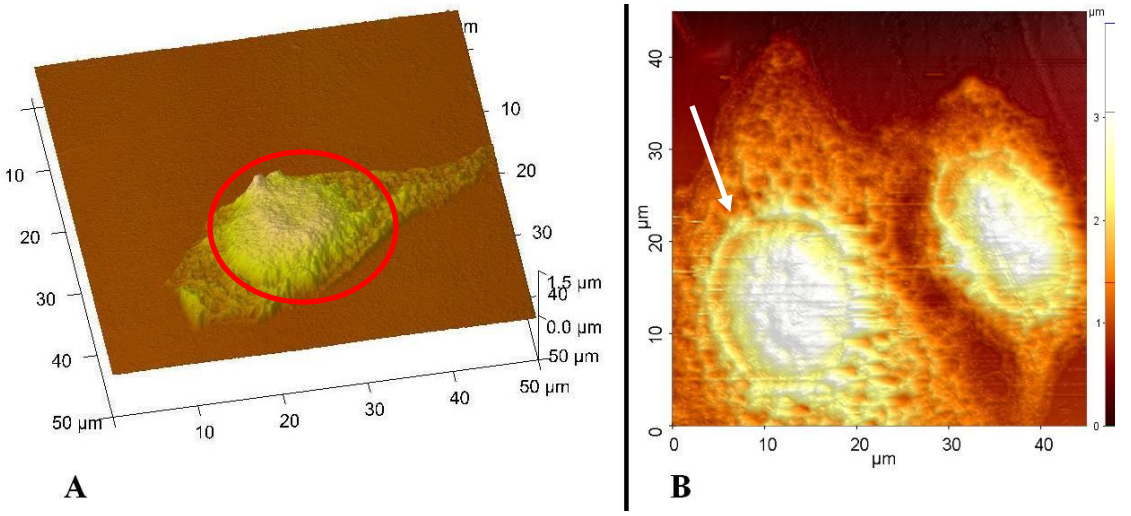

FIGURE 10 – Control Cells Fixation Comparison

(A) Osmium tetroxide fixed cell. (B) Methanol fixed cells.

the control group and was not infected with RSV. Figure 10B shows two methanol fixed control cells, and the vast similarities between topography images of cells fixed with either procedure served as the justification for the use of methanol fixation for this experiment.

Uninfected cells exhibit an internal nuclear structure of a rounded bulge (circled in figure 10A) bordered distinctly by the nuclear envelope (arrow in Figure 10B). The boundary between nucleus and cytoplasm is readily discerned upon inspection as is the edge of the cellular membrane. Figure 10B exhibits a higher concentration of circular volcano-like depressions in the cell membrane than the cells fixed with osmium tetroxide. This is likely attributed to the higher degree of dehydration during the fixation process resulting from the use of methanol (Moloney, McDonnell, and O'Shea 2004a). These depression artifacts have been observed in methanol-acetone fixative mixtures as well as methanol solutions in other work (Hahm and Anderer 2006; Hoetelmans et al. 2001). When cells infected by RSV for several hours and fixed with methanol were compared to

those fixed with osmium tetroxide, it appeared that the number of circular depressions in the cytoplasm was significantly higher in the methanol-fixed cells. The number of depressions increased but the average depth remained comparable when comparing control and infected cells fixed with methanol. Glutaraldehyde and osmium tetroxide fix cellular proteins and lipids in mechanisms limited by the reaction rate, whereas methanol fixation and subsequent dehydration of cells occurs as a function of transport into the cell through the membrane. Destruction and alteration of the cellular membrane from RSV infection is likely to increase the diffusion rate of methanol across the cellular boundary, resulting in a higher presence of depression artifacts for longer periods of viral infection.

Images obtained from methanol-fixed cells after 0, 4, and 24 hours of incubation with the respiratory syncytial virus comprise Figures 10, 11, and 12 respectively. The nuclear envelope is very distinct in the control cells that were not exposed to RSV as denoted in Figure 10B. The ring itself is identified as the edge of the nuclear membrane that, being more rigid than the cellular membrane, appears significantly raised above the cytoplasm of the cells around the nucleus perimeter. The circular depression concentric to but immediately inside the nuclear envelope (designated with an arrow in Figure 10B) is where the membrane sags slightly below the rigid edge resulting in a small valley. The large amorphous mound at the center of the nucleus is comprised of the nuclear envelope, chromatin, and nucleoli and marks the maximum height of the cell. The internal structures of the nucleus remain indistinguishable with any certainty but small peaks in the image might suggest possible locations. The slightly lower area immediately surrounding the cell nucleus likely demarcates the presence of cytoplasmic organelles including the endoplasmic reticulum and mitochondria.

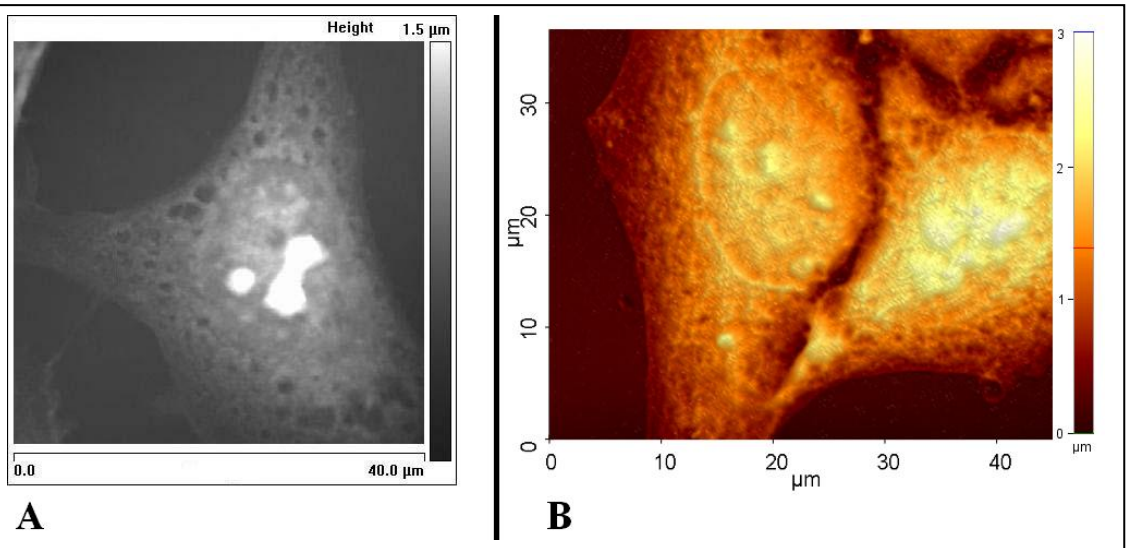

Figure 11 – RSV Infected Cells Fixation Comparison

(A) Osmium tetroxide fixed 4hrs of incubation with RSV. (B) Methanol fixed cells, 4hrs of incubation with RSV.

Cells incubated with the virus for a period of 4 hours prior to fixation exhibit some noticeable changes in structure made apparent by the atomic force microscope. The perimeter of the nuclear membrane is noticeably less defined and large craters or gaps begin to appear in its structure. It becomes more difficult to differentiate from the rest of the cell but its relative position can still be estimated based on the increased height of the nuclear region as compared to that of the cytoplasm. Inner nuclear structures begin to resolve out of the topographical images as smaller dome-like peaks within the bulge of the nucleus. These structures represent the most rigid components that are able to withstand the collapsing pressures of the cell during the dehydration process. Figure 11 shows HEp-2 cells exhibiting such characteristics in close proximity.

Cells imaged after incubation for a period of 24 hours (Figure 12) reveal further developments of the characteristics present in cells infected for shorter periods of time. The most notable development in cellular structure is found in the cytoplasm of the cell bodies. The holes and depressions in the cytoplasm are found in a much greater quantity

than those of the control cells suggesting that even more cytoplasmic material has been removed from the effects of the RSV infection. The pitting is even visible inside the boundary of the deteriorating nuclear membrane suggesting a very significant decrease in the volume of the cell. This decrease in volume varies directly with viral incubation time and in line with the observations made by Lee.

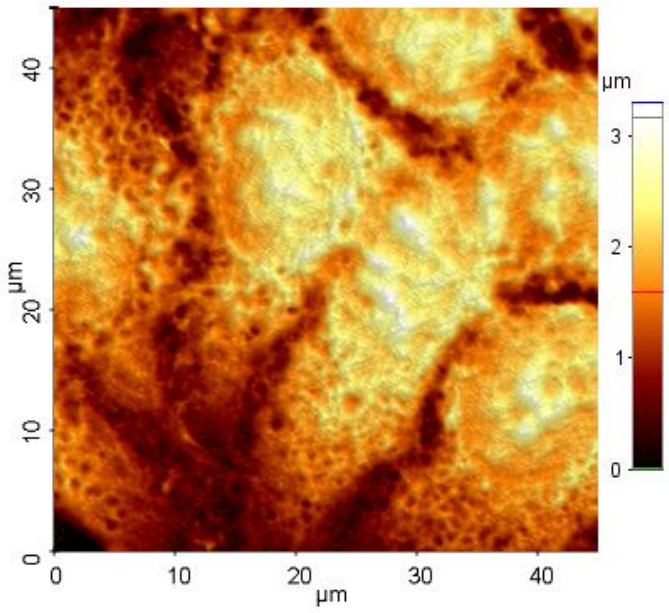

FIGURE 12 – Methanol Fixed 24hr RSV Infection Cells

The nuclear envelopes have deteriorated substantially and sometimes are barely discernable from the cytoplasm. The nuclear peaks protrude more than 800nm on average above the surrounding nucleus and are more defined than those visible in Figure 11. It is known that RSV replicates completely within the cell cytoplasm and is able to multiply in enucleated cells (Collins and Murphy 2001). The most apparent changes observed by the AFM occur in the cell nucleus which plays no part in the reproductive cycle of the virus. Two different postulates have been formed in order to explain the observed nuclear changes, specifically the collapse of the majority of the cell nucleus around the most rigid structures. The structural alterations may be attributed to the formation of an osmotic gradient and/or overall cellular collapse.

Exocytosis of the replicated RSV virions not only removes a portion of the host cell cytoplasm but also coats the vesicle by removing an area of the host cell plasma membrane (Collins and Murphy 2001). As the viral replication progresses, increasing amounts of cytoplasm exit the cell which may create an osmotic gradient between the nucleus and cytoplasm. The higher osmotic pressure within the nucleus forces water out through the nuclear envelope to establish an equilibrium pressure in the cytoplasm. This increasing loss of pressure within the nucleus would cause the nuclear envelope to collapse and expose the most rigid nuclear structures as seen in Figure 12.

In the proposed mechanism of cellular collapse, the RSV infection removes sections of the plasma membrane faster than it is able to be repaired and replaced by the host cell. This rampant exocytosis would result in the formation of large holes in the plasma membrane causing cytoplasm to leak out into the extracellular space. This loss of volume would also induce an osmotic pressure gradient between the nucleus and the rest of the cell but would ultimately result in the collapse of the entire cell. The sinking of the plasma membrane would be prevented at sites where the organelles and internal nuclear structures are the most rigid, significantly increasing their detection by topographical imaging techniques. It is likely that some combination of both mechanisms occurs throughout the duration of the infection and results in the clear imaging of structures not appearing in control cells. Figure 13 shows images of only methanol fixed cells after 0, 4, 8, and 24 hours of exposure to the respiratory syncytial virus exhibiting such characteristics attributed to the viral infection.

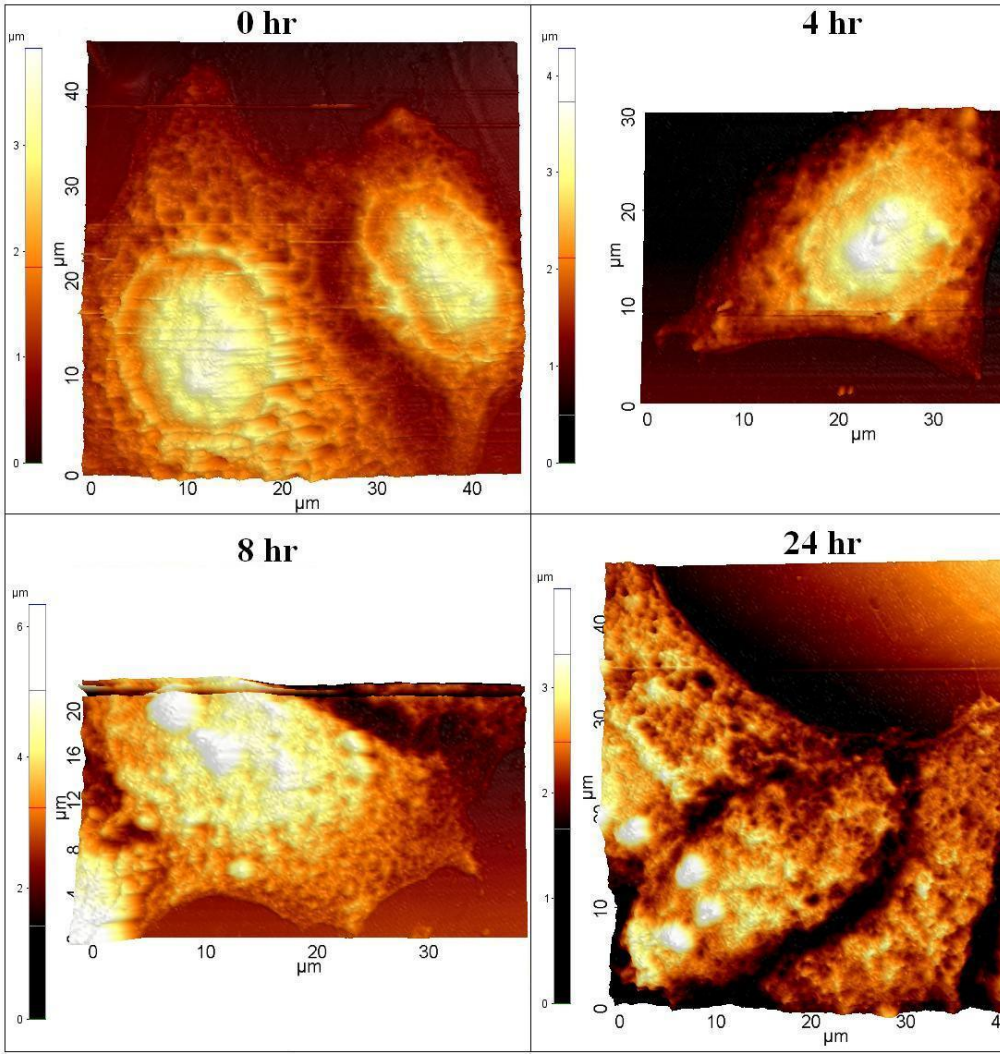

FIGURE 13 – Methanol Fixed Cells Imaged at 0, 4, 8, and 24 hours of Infection

2. RSV Imaging

Initial NC-AFM imaging of RSV adhered to an atomically smooth mica surface shows structures with an average height of 85.2 +/- 0.9nm. This is in good agreement with the round and filamentous forms of RSV found to be 80-100nm in diameter (Roberts, Compans, and Wertz 1995). Individual viruses appear as round circles in Figure 14, with the more irregular shapes belonging to agglomerated viral structures.

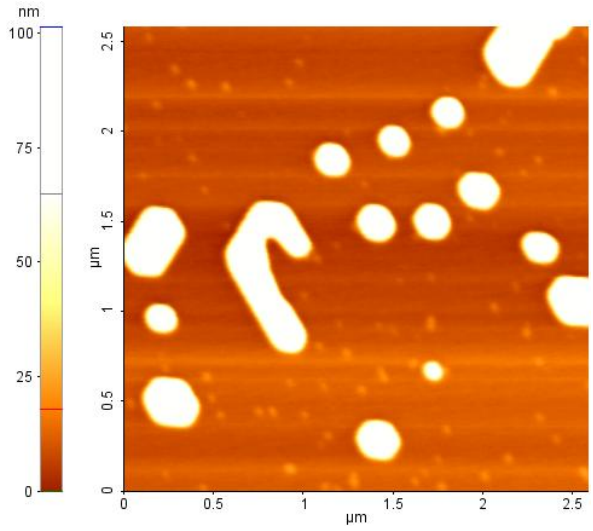

FIGURE 14 – NC-AFM RSV Image

B. Force-Distance Spectroscopy Results

1. Elastic Deformation Check

In order to measure the elastic modulus of any substance, the underlying assumption is that the material when subjected to a force will deform and then return to its original configuration when the force is removed. The measure of how much deformation occurred due to a given stress is used to determine the component elastic modulus. If the material were to irreversibly change from the applied force this resulting plastic deformation would render the elastic modulus incalculable for that magnitude of force. Preliminary force-distance spectroscopy indentions were repeated on a single

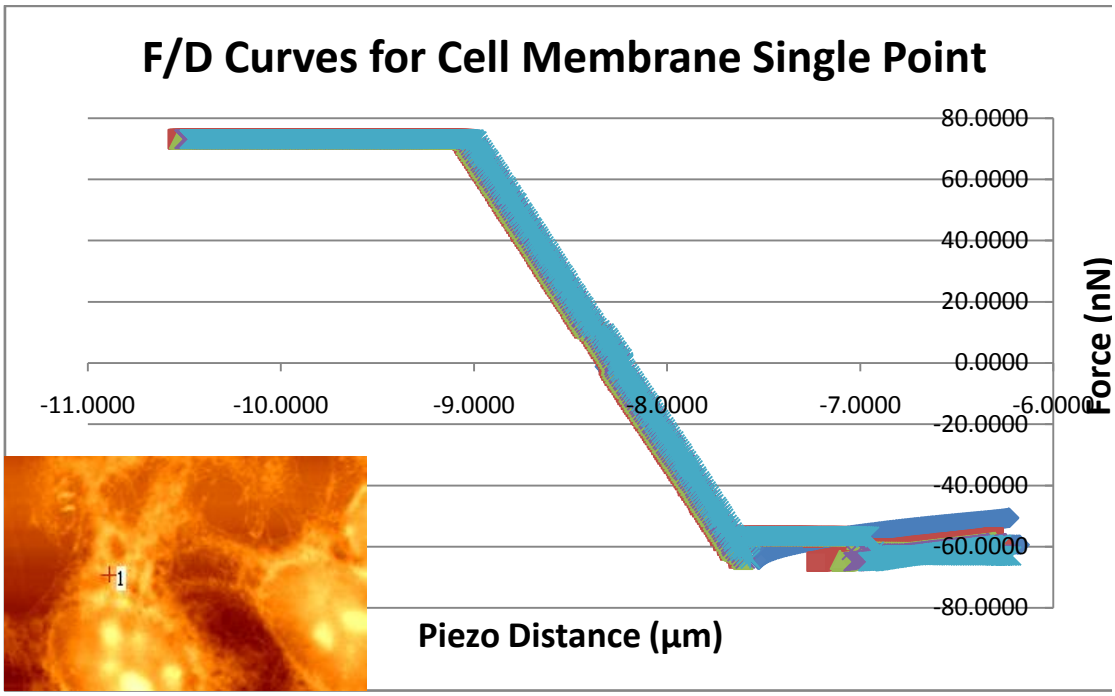

FIGURE 15 – Elastic Deformation Check Graph

point in order to make sure that no plastic deformations occurred in the cell cytoplasm, nucleus, or nuclear peaks in the force range of interest, 0-99nN. If the approach and retraction curves are approximately the same, and are reproducible after repeated indentations in a single location, then the sample deformation is elastic and a modulus of elasticity may be calculated (Radmacher 2002). Figure 15 shows five nearly identical approach and retraction curves taken at a single point on a cellular membrane shown in the inset image. The very high similarity and reproducibility of these curves indicate elastic deformation of the cell membrane during force-distance spectroscopy study, and this was found to hold true for points inside the nucleus including nuclear peaks.

2. Elastic Modulus Analysis

Force-distance curves were generated on at least 250 different locations spanning a minimum of eight different cells for all durations of RSV infection studied. The elastic modulus for each point was calculated from a first order regression fit of the data

acquired after tip contact with the sample surface. The slope of the regression line was fitted to the data acquired from the first 200nm of indentation in order to minimize the effect of the substrate on elasticity measurements. The presence of a hard substrate beneath the cells would be expected to influence the force-distance curve data for penetration depths greater than 10% of the height of the cell samples (Jung et al. 2004). When indentation data for cells was compared to data for a blank cover slip, it was noticed that the cover slip is only slightly harder than the cells being studied further reducing its effect on the acquired data. The effects of the substrate were not noticed in most indentations even up to 50% of the sample height. Only regression lines with an R^2 of 0.9 or greater were used to calculate a modulus of elasticity, and then outliers were removed based on Chauvenet's criterion.

TABLE I

ELASTIC MODULUS RESULTS

Infection Duration (hrs)	0	0.5	4	8	16	24
Number of Points	245	231	242	272	258	257
Standard Deviation	0.946	0.570	0.280	1.914	0.167	0.273
Elastic Modulus (kPa)	**1.146**	**0.798**	**0.747**	**1.493**	**0.535**	**0.618**

It can be seen in TABLE I that the average elasticity for all cells studied at a given length of RSV infection do not have a strong correlation. The reported elastic modulus calculated at eight hours of infection is particularly suspect since the value of the standard deviation for this data set is larger than the reported elastic modulus. The value calculated for the control sample also possesses a very large standard deviation reducing the accuracy of this measurement. Histograms showing all the data

distributions can be found in Appendix I. Figure 16 shows a graph displaying all of the data points collected as well as the reported values for the average elastic modulus at each period of infection from Table I. Based on the results of extrapolation by norm approximation to detect a trend in the data, the elastic moduli cannot conclusively be said to decrease as the duration of the RSV infection lengthens. This method fits the data with polynomial curves of moderate degrees (from three to eleven in this case) and uses the fitted function to predict the value of a data point immediately outside of the data set. If the predicted point is consistently lower than the average value of the data taken at the last interval (24hr infection data in this case) then the probability that the data exhibits a decreasing correlation is very high. This method is often used in order to determine if a trend exists and in which general direction it is moving but is only valid if any existing

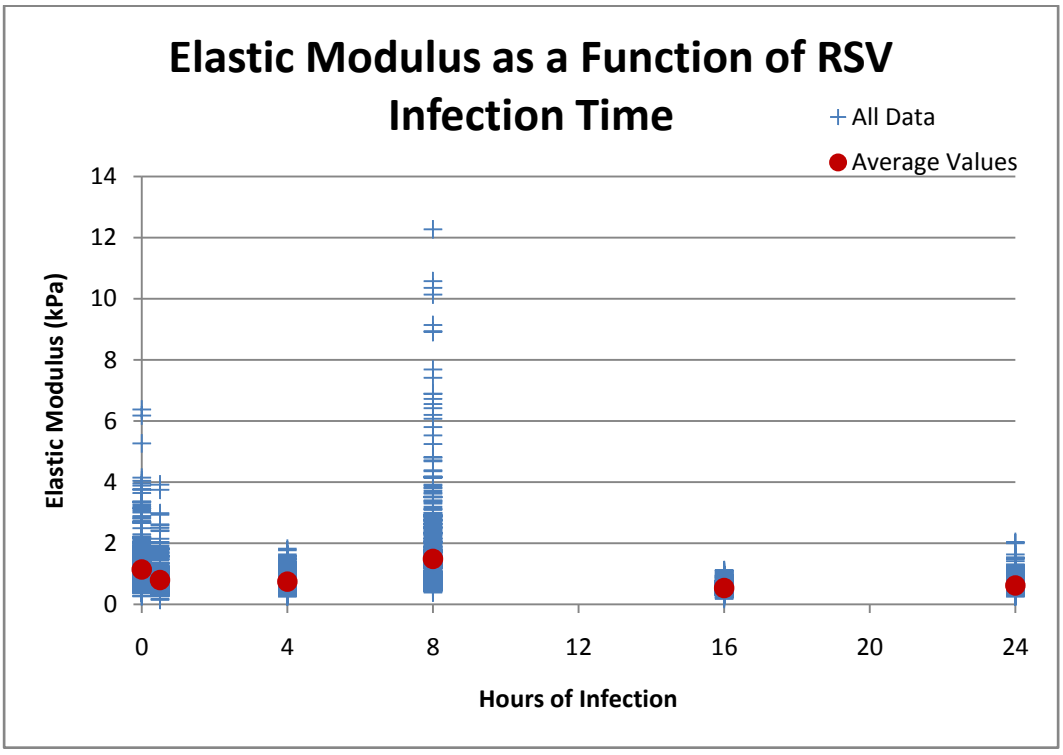

FIGURE 16 – Elastic Modulus Trend Graph

trend holds true outside of the observed interval. This should be the case in this experimental setup, as the mechanical properties of cells infected by RSV should not be drastically different if they were infected for slightly more than 24 hours.

In order to determine if the actin structures making up the cytoskeleton degrade as a result of the replication of the respiratory syncytial virus, elasticity analysis should be performed on unfixed, living cells. This hypothesis should be tested by work done on living cells so as to remove any potential fixation effects which likely mask any trend in the data if it exists at all. Fixation processes kill and preserve cells by forcing the condensation or cross-linking of cellular components which will affect the actin cytoskeleton. Performing a similar experiment on living cells would serve to validate or refute this hypothesis more strongly than futher study using different fixative agents which all alter the mechanical properties of cells.

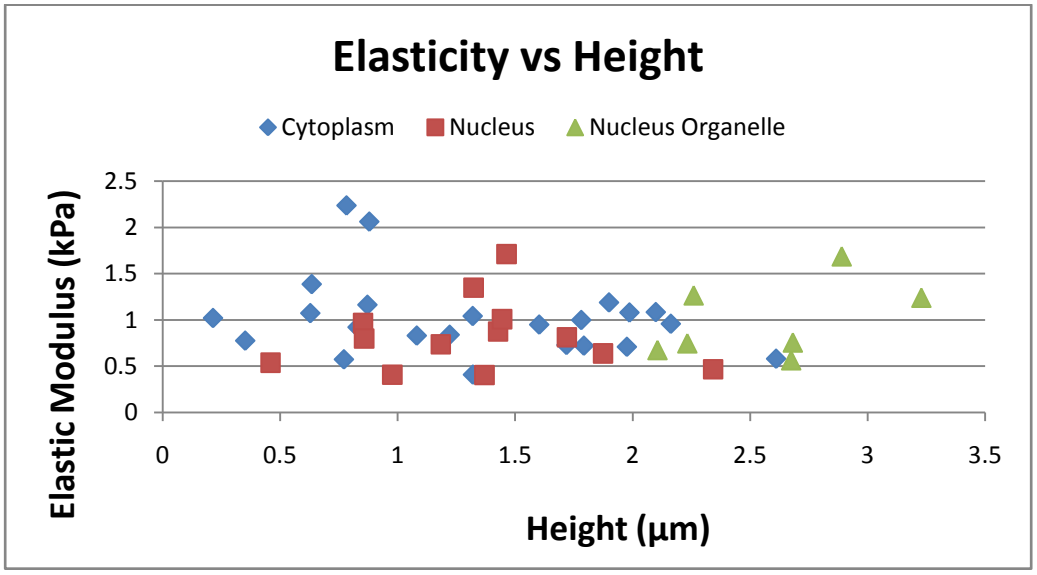

FIGURE 17 – Elastic Modulus vs. Sample Height Graph

Data displayed in this graph was acquired from a single control cell, and the height at the approximate location of indentation was measured for comparison.

3. Individual and Intracellular Elasticity Analysis

It was thought that determination of the elastic modulus may be influenced by the amount of material present in the studied location more so than by the structure of the actin cytoskeleton present. In order to test for any sort of dependence on height, an individual control cell was indented, and the height at each of the 45 different locations was measured using the XEI software. The heights of the points that were indented ranged from about 200nm up to 3.2μm. The elastic modulus for the cell cytoplasm was calculated as 1.01kPa with an average height of 1.31μm. The modulus of elasticity calculated for the nucleus was 0.88kPa at an average height of 1.77μm. It is of interest to note that the average elastic modulus of the nucleus was heavily influenced by the moduli of the highest points. The elastic modulus at these points was calculated at 0.99kPa as compared to 0.83kPa for all other areas inside the nuclear envelope. Figure 17 displays elastic modulus data graphed against the cellular height at the site of indentation and broken into three subcategories based on location: cellular membrane, nucleus, and nuclear peaks. From this data it is apparent that no strong correlation exists and that the elastic modulus at any point is largely independent of the sample height but relies more heavily on the underlying supporting structures especially when comparing points in the cytoplasm to those within the nucleus.

In order to further test for the apparent link between cell elastic modulus and relative location of indentation, further analysis was conducted on the data provided by all the control cells studied. Data from 126 indentations in cell membranes were compared to that obtained from 119 force-distance curves taken in cell nuclei for nine different cells. The elastic modulus for all the membrane data was calculated as 1.5kPa

and 1.1kPa for the nuclei data. The nucleus was indented at random points spread throughout its interior. The smaller modulus of elasticity indicates that the nucleus is more readily deformable than the cell membrane, supporting the postulates formed to explain the presence of the raised structures inside the nuclear envelope occurring after infection with RSV.

4. Hydrophobic Membrane Analysis

TABLE II

ADHESION FORCE RESULTS

Infection Duration (hrs)	0	0.5	4	8	16	24
Number of Points	245	231	242	272	258	257
Standard Deviation	0.946	1.337	1.617	1.391	1.903	1.26
Adhesion Force (kPa)	**11.735**	**10.117**	**9.320**	**7.780**	**10.470**	**7.449**

As seen in TABLE II, the adhesion force immediately prior to the membrane-tip detachment steadily decreases as the RSV infection progresses. Histograms of the data distributions for adhesion forces can be found in Appendix II. Since this force depends on the concentration of hydrophobic molecules expressed by the cellular membrane, this correlation describes a decrease in the presence of these molecules or an increase in the hydrophilic nature of the membrane resulting from the RSV infection. This change in chemical makeup is most likely attributed to the exocytosis of RSV virions that remove a portion of the cell membrane as they exit. Rapid removal of the existing cell membrane may dramatically alter the molecules expressed in the extracellular matrix as the cell begins to repair and replace the missing lipid bilayer. Figure 18 shows the decrease in

hydrophobicity of the cell membrane as a function of RSV infection progression. This trend was validated through results obtained from extrapolation by norm approximation for polynomial fits of the data.

Hydrophobicity of cell membranes have been reported to be one of the primary forces involved in the adhesion of pathogens to cellular surfaces (Dague et al. 2007). The regulation of hydrophobic or hydrophilic molecule concentration on cell surfaces emerges as a potential area of interest for the inhibition of respiratory syncytial virus infection. Even if controlling the hydrophobicity of a cell membrane does not prove to be a feasible method of moderating the infection, it may potentially be used to monitor the progress of the RSV infection in further studies.

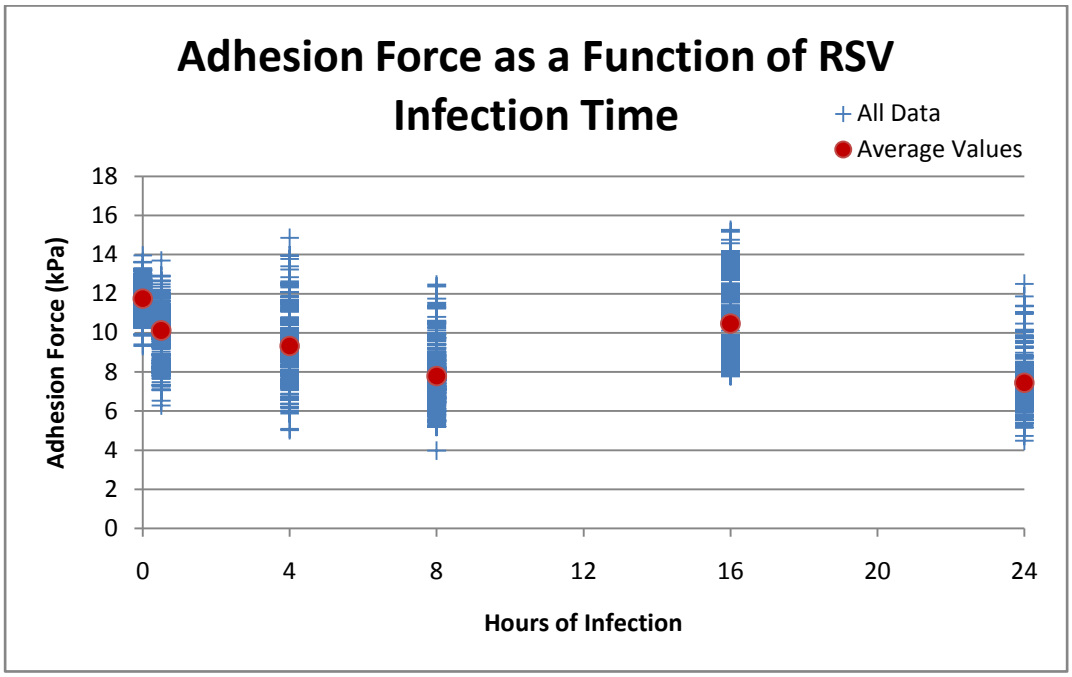

FIGURE 18 – Adhesion Force Trend Graph

IV. CONCLUSIONS

Atomic force microscopy is a versatile and valuable tool for the analysis of changes in the physical characteristics and three dimensional structure of HEp-2 cells infected by the human respiratory syncytial virus. The use of methanol as a primary fixative results in several adverse affects on the cellular structure and physical characteristics including protein extraction, swelling of the entire cell and nucleus, and the presence of depression artifacts. When obtained images were compared to images of HEp-2 cells fixed with glutaraldehyde and osmium tetroxide solutions, the characteristics of the viral infection remained consistent. The presence of significant circular depressions, deterioration of the nuclear membrane, and protrusion of inner-nuclear structures all progress for up to 24 hours of infection and can be observed as early as 4 hours when compared to healthy cells. It is likely that the protrusion of the nuclear structures does not result directly from viral interaction but instead is created from a sizable volumetric loss from the cytoplasm due to rampant exocytosis of the virions. The observed decrease in the height of the cell membrane and the nuclear membrane for cells fixed by osmium tetroxide was not confirmed in the AFM analysis of the methanol fixed cells. While methanol is readily accessible and significantly cheaper than many other fixatives, it is recommended that studies of fixed cells depending on the analysis of cellular structure, size, or the concentrations of cellular proteins use a solution of glutaraldehyde followed by osmium tetroxide to minimize the distortion of the living cell structure prior to analysis.

The elastic modulus of methanol-fixed HEp-2 cells was found not to decrease during the infection and replication of the respiratory syncytial virus for durations up to 24 hours. It has been reported that RSV does not cause structural changes to the actin cytoskeleton, and this has been corroborated during the first day of infection in this study using fixed cells. In order to more conclusively determine the impact of the virus on the structural matrix of cells, further work should be done on live cells in order to remove the reportedly significant distortion from the fixation process. The elastic modulus of an individual cell nucleus was found to be consistently higher than that of its cytoplasm and is independent of the height of the cell at the point of indentation. The elastic moduli at the tallest nucleus locations were determined to be larger than that for the surrounding areas. The larger moduli for the tallest regions imply that as the volume of the nucleus decreases, the nuclear envelope is supported by the more rigid internal structures and sags where they are absent corroborating the qualitative observations of the images before indentation analysis occurred. The hydrophobicity of the surface of the cell membrane steadily decreases during the RSV infection for up to 24 hours either through removal of hydrophobic molecules or the heightened expression of hydrophilic groups. This change is likely attributable to the rapid removal and repair of the lipid bilayer and might be useful to measure the progression of the viral infection. Further study should be made to observe the effects of the respiratory syncytial virus on live HEp-2 cells to establish definitive trends and also to further quantify the influence of fixatives on the mechanical properties of infected cells.

REFERENCES

Albrecht, T. R., S. Akamine, T. E. Carver, and C. F. Quate. 1990. Microfabrication of cantilever styli for the atomic force microscope. *Journal of Vacuum Science & Technology a-Vacuum Surfaces and Films* 8, no. 4: 3386-3396.

American Lung Association. Respiratory syncytial virus fact sheet. http://www.lungusa.org/site/pp.asp?c=9oICLOOxGrF&b=1541257 (accessed 1-25-2009.

AppNano. Appnano probe features. http://www.appnano.com/pdf/Probe_Intro.pdf (accessed 2-9-2009.

ATCC. Ccl-23 product description. http://www.atcc.org/ATCCAdvancedCatalogSearch/ProductDetails/tabid/452/Default.aspx?ATCCNum=CCL-23&Template=cellBiology (accessed 2-20-2009.

Binnig, G., C. Gerber, E. Stoll, T. R. Albrecht, and C. F. Quate. 1987. Atomic resolution with atomic force microscope. *Europhysics Letters* 3, no. 12: 1281-1286.

Binnig, G., C. F. Quate, and C. Gerber. 1986. Atomic force microscope. *Physical Review Letters* 56, no. 9: 930-933.

Bourne, G. H., J. F. Danielli, and Kwang W. Jeon. 1969. *International review of cytology*: Academic Press.

Boyoglu, Seyhan, Komal Vig, Adam Pfendt, Shreekumar Pillai, Gerold Willing, and Shree Singh. 2009. Analysis of the effect of gold and silver nanoparticles on rsv using afm. *Nano Science and Technology Institute*.

Braet, F., C. Rotsch, E. Wisse, and M. Radmacher. 1998. Comparison of fixed and living liver endothelial cells by atomic force microscopy:S575-S578.

Butt, H. J., B. Cappella, and M. Kappl. 2005. Force measurements with the atomic force microscope: Technique, interpretation and applications. *Surface Science Reports* 59, no. 1-6: 1-152.

Butt, H. J., P. Siedle, K. Seifert, K. Fendler, T. Seeger, E. Bamberg, A. L. Weisenhorn, K. Goldie, and A. Engel. 1993. Scan speed limit in atomic force microscopy. *Journal of Microscopy-Oxford* 169: 75-84.

Center for Disease Control. 2004. Brief report: Respiratory syncytial virus activity. In *Morbidity and Mortality Weekly Report*:Vol 53(49).

_____. Respiratory syncytial virus infection. http://www.cdc.gov/rsv/about/infection.html (accessed 1-23-2009.

Cleveland, J. P., S. Manne, D. Bocek, and P. K. Hansma. 1993. A nondestructive method for determining the spring constant of cantilevers for scanning force microscopy. *Review of Scientific Instruments* 64, no. 2: 403-405.

Collins, P. L. and B. R. Murphy. 2001. *Fields virology*. Edited by B. N. Fields. Philadelphia, PA: Lippincott Williams & Wilkins.

Dague, E., D. Alsteens, J. P. Latge, C. Verbelen, D. Raze, A. R. Baulard, and Y. F. Dufrene. 2007. Chemical force microscopy of single live cells. *Nano Letters* 7, no. 10: 3026-3030.

Dufrene, Y. F. 2008. Afm for nanoscale microbe analysis. *Analyst* 133, no. 3: 297-301.

Easton, Andrew. Rsv graphic depiction. http://template.bio.warwick.ac.uk/staff/easton/IMAGES/Diagrams/3dvirus.jpg (accessed 1-25-2009.

Erlandsson, R., G. Hadziioannou, C. M. Mate, G. M. McClelland, and S. Chiang. 1988. Atomic scale friction between the muscovite mica cleavage plane and a tungsten tip. *Journal of Chemical Physics* 89, no. 8: 5190-5193.

Hahm, D. and U. Anderer. 2006. Establishment of hep-2 cell preparation for automated analysis of ana fluorescence pattern:178-181.

Heinz, W. F. and J. H. Hoh. 1999. Relative surface charge density mapping with the atomic force microscope. *Biophysical Journal* 76, no. 1: 528-538.

Henderson, E., P. G. Haydon, and D. S. Sakaguchi. 1992. Actin filament dynamics in living glial-cells imaged by atomic force microscopy. *Science* 257, no. 5078: 1944-1946.

Hertz, H. and J. Reine. 1882. *Angew. Math.* 92: 156.

Hoetelmans, R. W. M., F. A. Prins, I. Cornelese-ten Velde, J. van der Meer, C. J. H. van de Velde, and J. H. van Dierendonck. 2001. Effects of acetone, methanol, or paraformaldehyde on cellular structure, visualized by reflection contrast microscopy and transmission and scanning electron microscopy. *Applied Immunohistochemistry & Molecular Morphology* 9, no. 4: 346-351.

Jena, B. P. 2002. Fusion pore in live cells. *News in Physiological Sciences* 17: 219-222.

Jung, Y. G., B. R. Lawn, M. Martyniuk, H. Huang, and X. Z. Hu. 2004. Evaluation of elastic modulus and hardness of thin films by nanoindentation. *Journal of Materials Research* 19, no. 10: 3076-3080.

King, R. 2004. Gene delivery to mammalian cells by microinjection. *Methods of Molecular Biology* 245: 167-174.

Kopycinska-Muller, M., R. H. Geiss, and D. C. Hurley. 2006. Contact mechanics and tip shape in afm-based nanomechanical measurements. *Ultramicroscopy* 106, no. 6: 466-474.

Lee, Kyoung G. 2006. Characterization of changes in biological interfaces utilizing atomic force microscope. Master of Engineering, University of Louisville.

Lulevich, V., T. Zink, H. Y. Chen, F. T. Liu, and G. Y. Liu. 2006. Cell mechanics using atomic force microscopy-based single-cell compression. *Langmuir* 22, no. 19: 8151-8155.

Lyubchenko, Y., L. Shlyakhtenko, R. Harrington, P. Oden, and S. Lindsay. 1993. Atomic force microscopy of long DNA - imaging in air and under water. *Proceedings of the National Academy of Sciences of the United States of America* 90, no. 6: 2137-2140.

Mate, C. M., R. Erlandsson, G. M. McClelland, and S. Chiang. 1988. Atomic force microscopy studies of frictional forces and of force effects in scanning tunneling microscopy. *Journal of Vacuum Science & Technology a-Vacuum Surfaces and Films* 6, no. 3: 575-576.

Matsumoto, T., Y. Maeda, Y. Naitoh, and T. Kawai. 1999. High-resolution imaging of single-stranded DNA on mica surface under ultrahigh vacuum conditions by noncontact atomic force microscopy. *Journal of Vacuum Science & Technology B* 17, no. 5: 1941-1945.

Moloney, M., L. McDonnell, and H. O'Shea. 2004a. Atomic force microscopy of bhk-21 cells: An investigation of cell fixation techniques. *Ultramicroscopy*, no. 100: 153-161.

_____. 2004b. Atomic force microscopy of bhk-21 cells: An investigation of cell fixation techniques:153-161.

Nath, Swapan Kumar and Sanjay G. Revankar. 2005. *Problem-based microbiology*: Elsevier Health Sciences.

Nicholson, K. G. 1996. Impact of influenza and respiratory syncytial virus on mortality in england and wales from january 1975 to december 1990. *Epidemiology and Infection* 116, no. 1: 51-63.

Obataya, F., C. Nakamura, S. W. Han, N. Nakamura, and J. Miyake. 2005. Mechanical sensing of the penetration of various nanoneedles into a living cell using atomic force microscopy:1652-1655.

Park Systems. Xe-100 product datasheet. http://www.parkafm.com/ (accessed 2-4-2009.

Putman, C. A. J., K. O. Vanderwerf, B. G. Degrooth, N. F. Vanhulst, and J. Greve. 1994. Viscoelasticity of living cells allows high-resolution imaging by tapping mode atomic-force microscopy. *Biophysical Journal* 67, no. 4: 1749-1753.

Radmacher, M. 2002. Measuring the elastic properties of living cells by the atomic force microscope. In *Atomic force microscopy in cell biology*, 68:67-90. San Diego: Academic Press Inc.

Radmacher, M., R. W. Tillmann, M. Fritz, and H. E. Gaub. 1992. From molecules to cells - imaging soft samples with the atomic force microscope. *Science* 257, no. 5078: 1900-1905.

Roberts, S. R., R. W. Compans, and G. W. Wertz. 1995. Respiratory syncytial virus matures at the apical surfaces of polarized epithelial-cells. *Journal of Virology* 69, no. 4: 2667-2673.

Rotsch, C., K. Jacobson, and M. Radmacher. 1998. *Scanning Micrsocopy* in press.

Sackmann, E. 1994. Intracellular and extracellular macromolecular networks - physics and biological function. *Macromolecular Chemistry and Physics* 195, no. 1: 7-28.

Seifert, U. and R. Lipowsky. 1995. *The structure and dynamics of membranes*. Edited by R. Lipowsky and E. Sackmann. Handbook of biological physics. Elsevier, Amsterdam.

Sen, S., S. Subramanian, and D. E. Discher. 2005. Indentation and adhesive probing of a cell membrane with afm: Theoretical model and experiments. *Biophysical Journal* 89, no. 5: 3203-3213.

Sirghi, L., J. Ponti, F. Broggi, and F. Rossi. 2008. Probing elasticity and adhesion of live cells by atomic force microscopy indentation. *European Biophysics Journal with Biophysics Letters* 37, no. 6: 935-945.

Sneddon, I. N. 1965. The relation between load and penetration in the axisymmetric boussinesq problem for a punch of arbitrary profile. *International Journal of Engineering Science* 3: 47-57.

Thompson, W. W., D. K. Shay, E. Weintraub, L. Brammer, N. Cox, L. J. Anderson, and K. Fukuda. 2003. Mortality associated with influenza and respiratory syncytial virus in the united states. *Jama-Journal of the American Medical Association* 289, no. 2: 179-186.

Vanlandingham, M. R., S. H. McKnight, G. R. Palmese, R. F. Eduljee, J. W. Gillespie, and R. L. McCulough. 1997. Relating elastic modulus to indentation response using atomic force microscopy. *Journal of Materials Science Letters* 16, no. 2: 117-119.

Weisenhorn, A. L., P. K. Hansma, T. R. Albrecht, and C. F. Quate. 1989. Forces in atomic force microscopy in air and water. *Applied Physics Letters* 54, no. 26: 2651-2653.

Wilson, M. 2002. *Nanotechnology basic science and emerging technologies*. Sydney, Australia: Chapman & Hall/CRC.

World Health Organization. 2005. State of the art vaccine research and development. WHO/IVB/05.XX.

APPENDIX I

ELASTIC MODULUS HISTOGRAMS

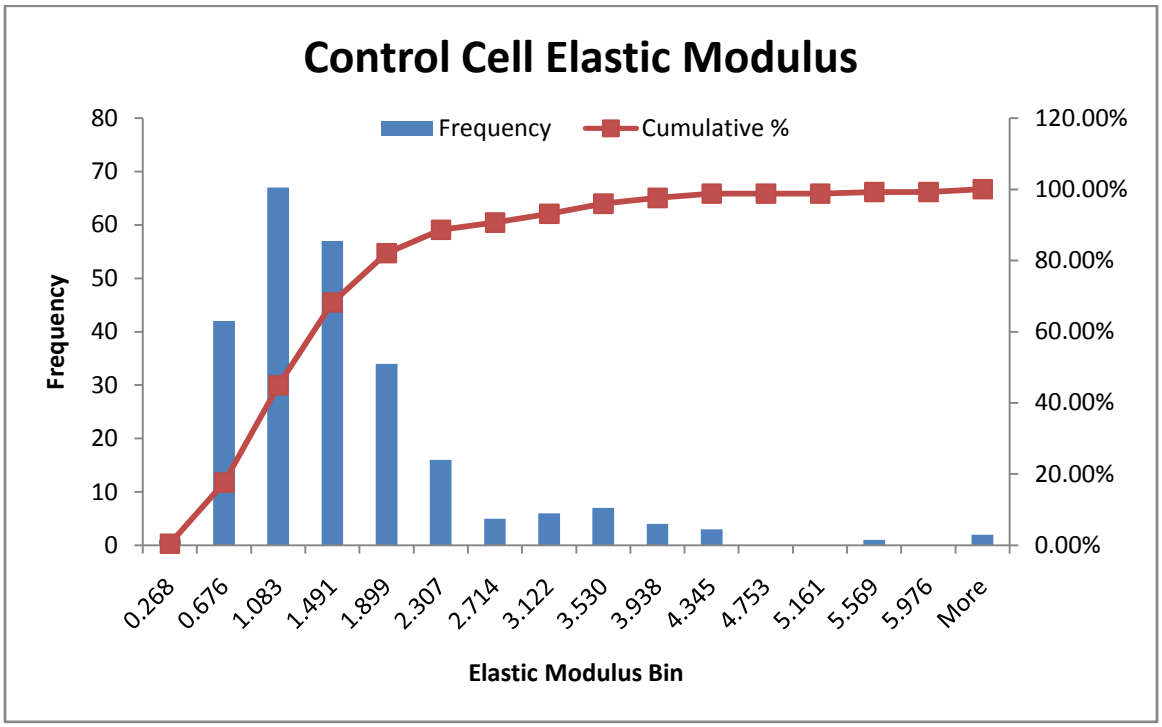

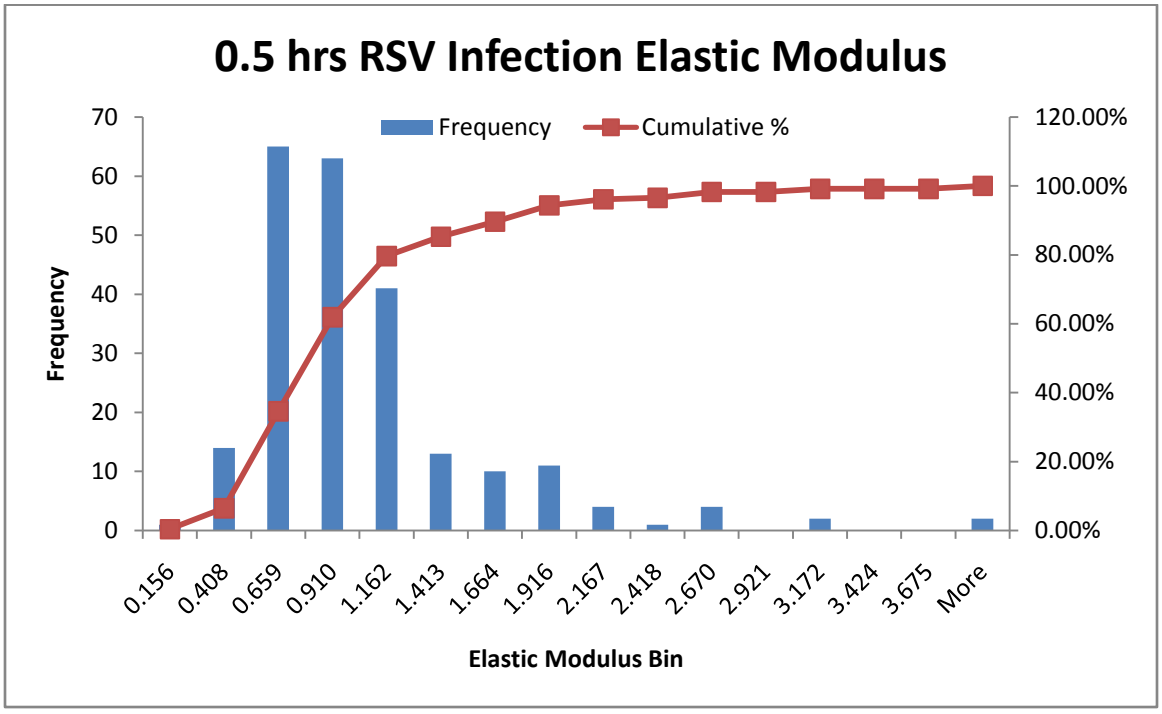

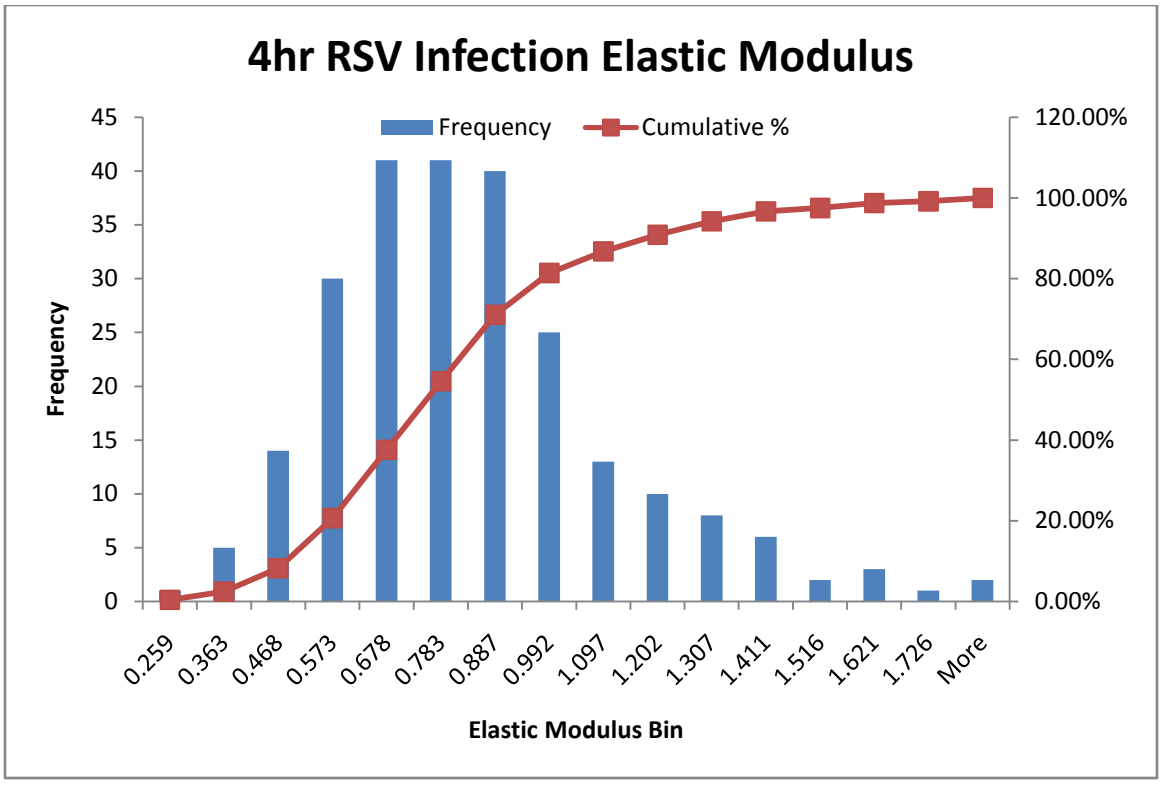
4hr RSV Infection Elastic Modulus
Frequency
Cumulative %
Frequency
Elastic Modulus Bin
0.259
0.363
0.468
0.573
0.678
0.783
0.887
0.992
1.097
1.202
1.307
1.411
1.516
1.621
1.726
More

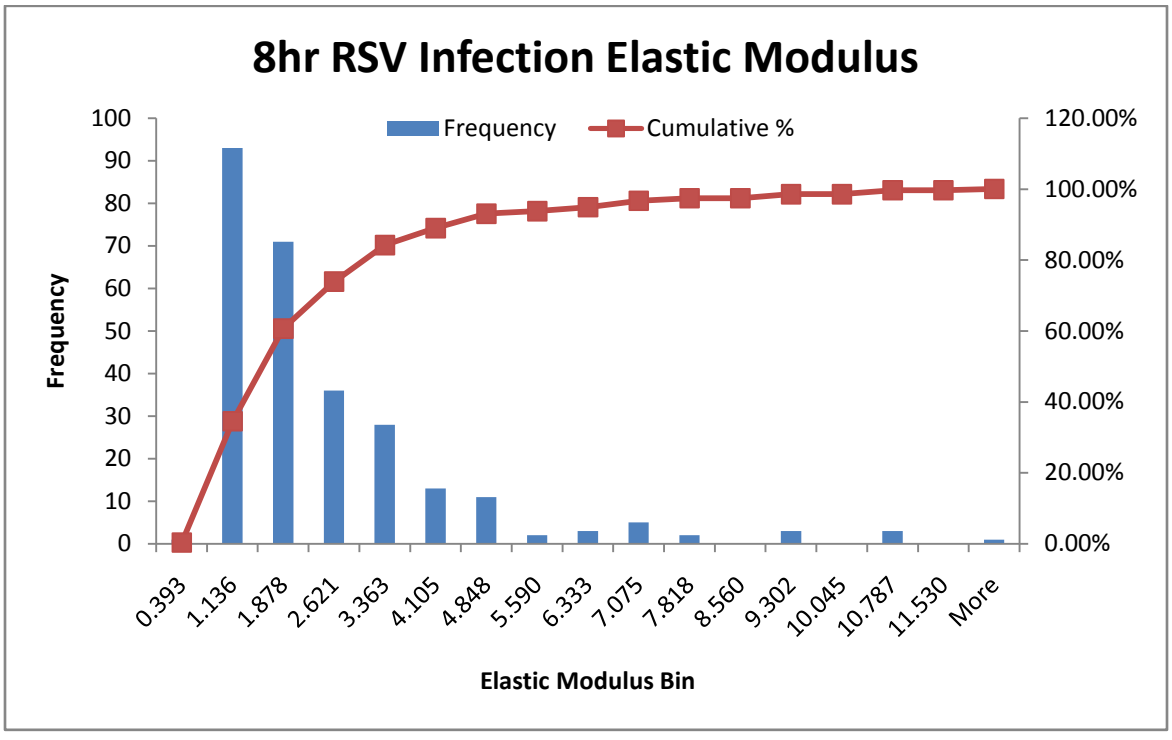
8hr RSV Infection Elastic Modulus
Frequency
Cumulative %
Frequency
Elastic Modulus Bin
0.393
1.136
1.878
2.621
3.363
4.105
4.848
5.590
6.333
7.075
7.818
8.560
9.302
10.045
10.787
11.530
More

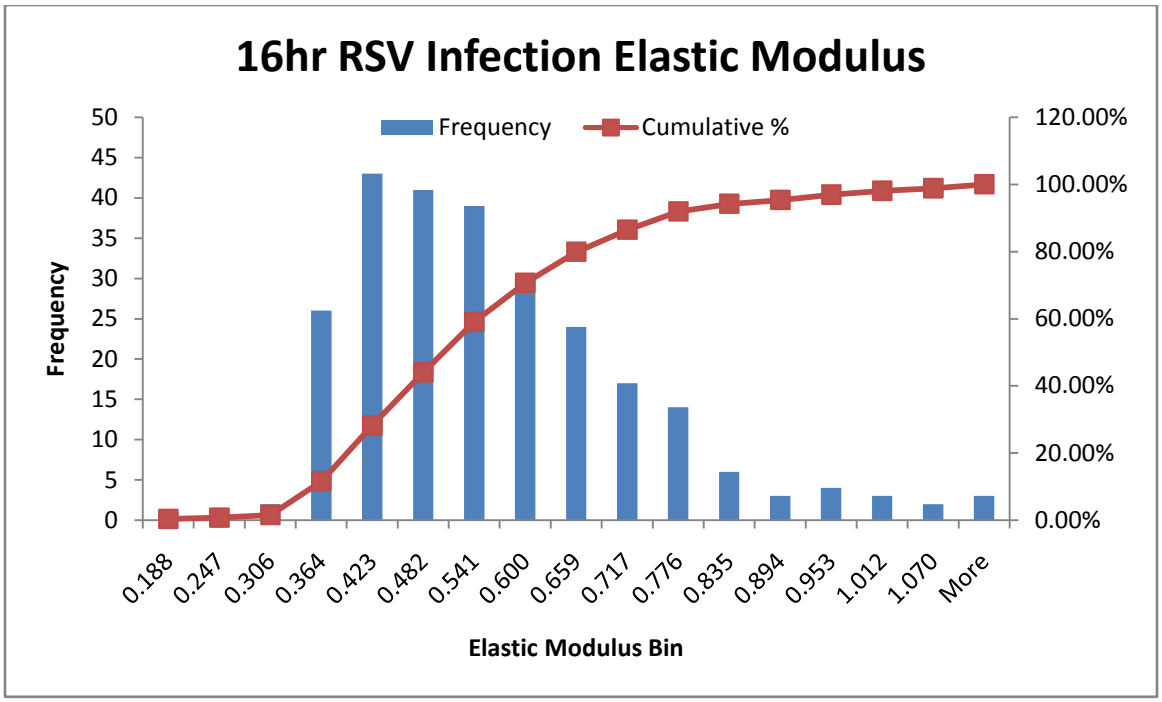
16hr RSV Infection Elastic Modulus
Frequency
Cumulative %
Frequency
Elastic Modulus Bin
0.188
0.247
0.306
0.364
0.423
0.482
0.541
0.600
0.659
0.717
0.776
0.835
0.894
0.953
1.012
1.070
More

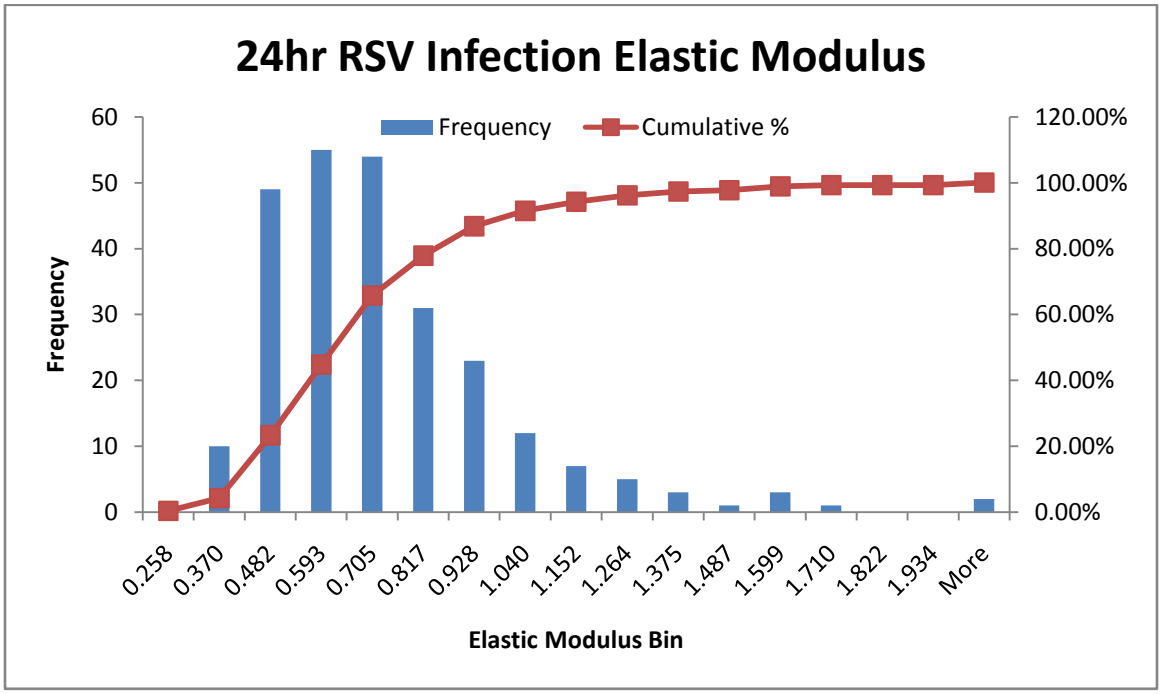
24hr RSV Infection Elastic Modulus
Frequency
Cumulative %
Frequency
Elastic Modulus Bin
0.258
0.370
0.482
0.593
0.705
0.817
0.928
1.040
1.152
1.264
1.375
1.487
1.599
1.710
1.822
1.934
More

APPENDIX II

ADHESION FORCE HISTOGRAMS

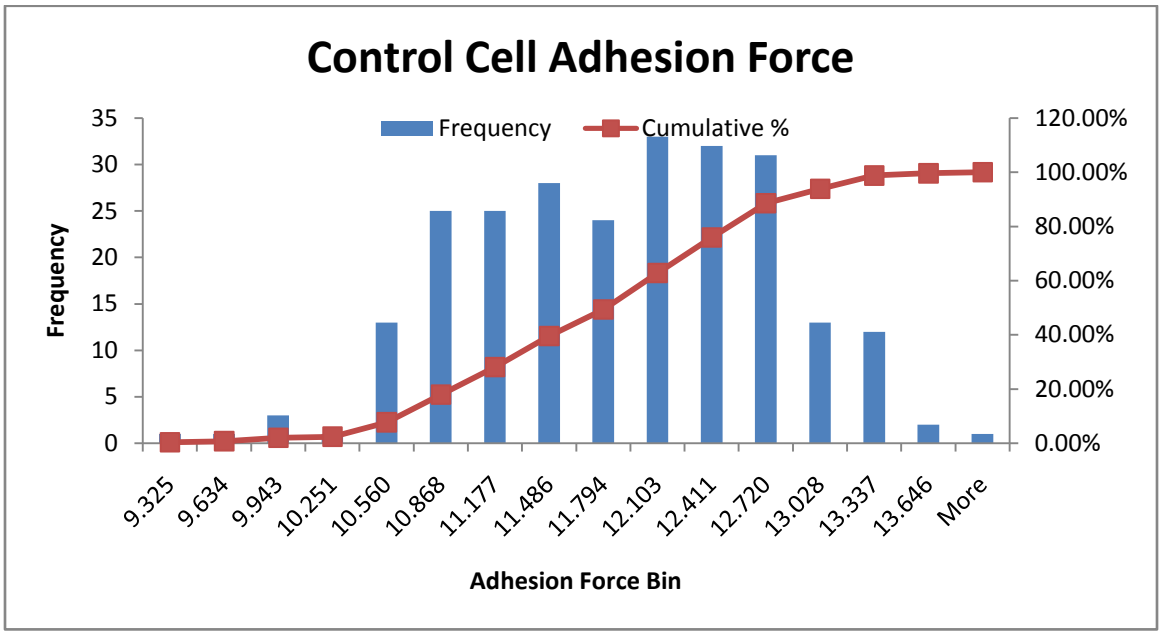

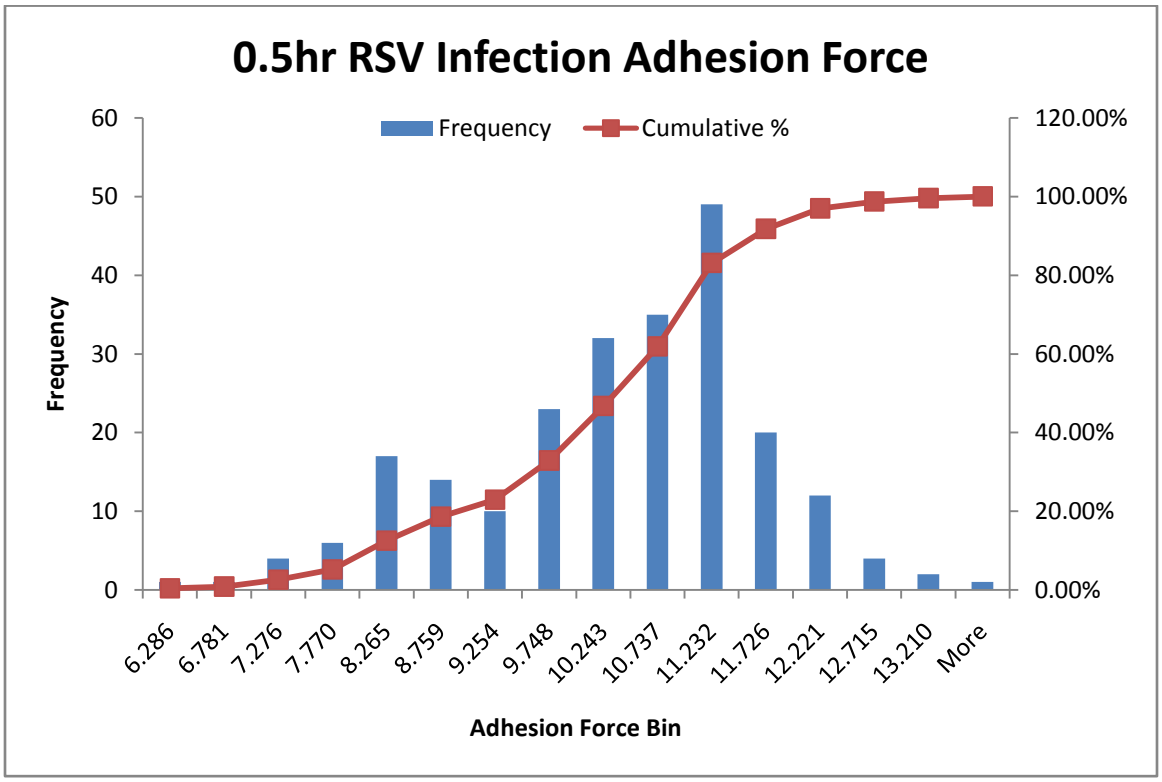

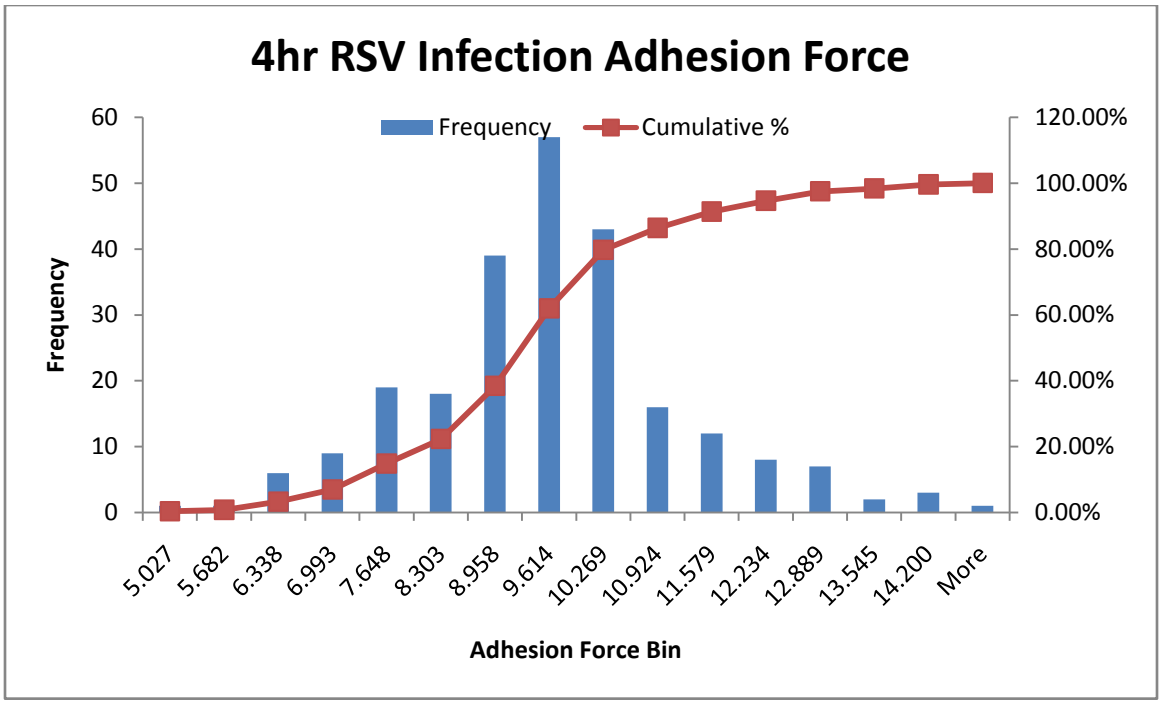
4hr RSV Infection Adhesion Force
Frequency
Cumulative %
Frequency
Adhesion Force Bin
0
10
20
30
40
50
60
0.00%
20.00%
40.00%
60.00%
80.00%
100.00%
120.00%
5.027
5.682
6.338
6.993
7.648
8.303
8.958
9.614
10.269
10.924
11.579
12.234
12.889
13.545
14.200
More

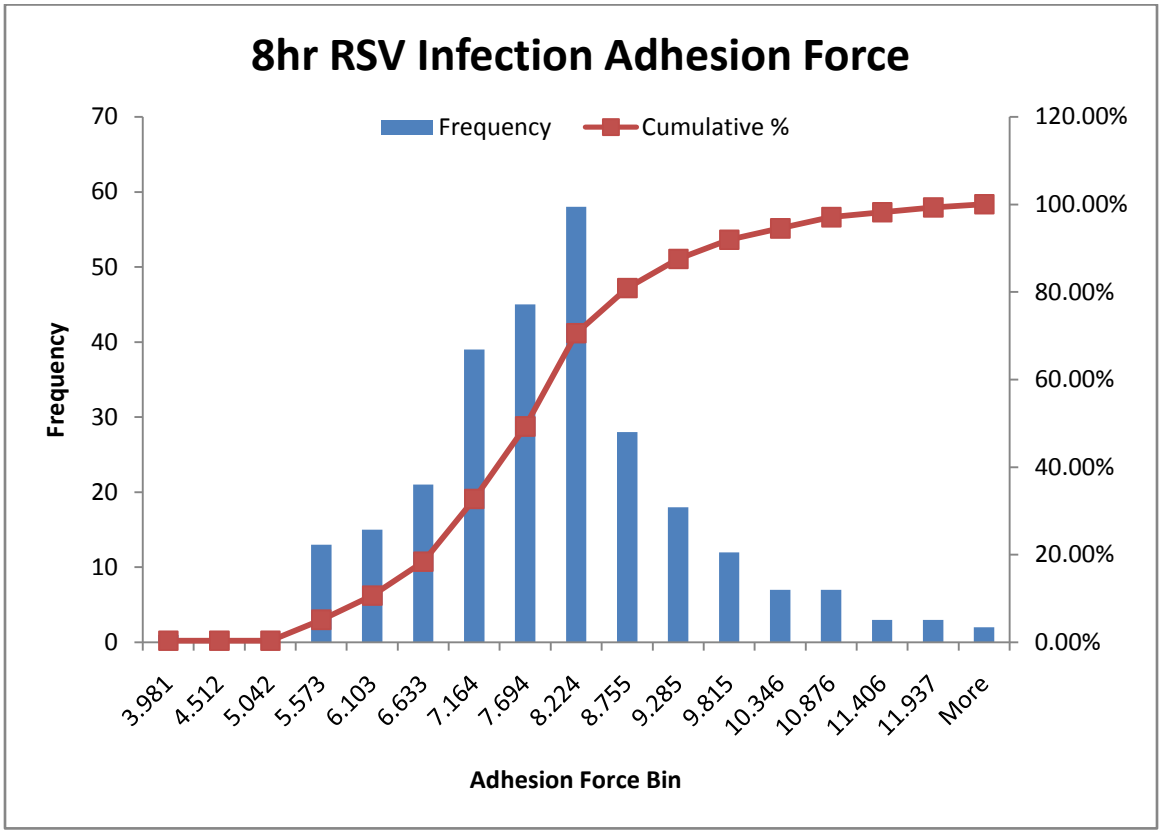
8hr RSV Infection Adhesion Force
Frequency
Cumulative %
Frequency
Adhesion Force Bin
0
10
20
30
40
50
60
70
0.00%
20.00%
40.00%
60.00%
80.00%
100.00%
120.00%
3.981
4.512
5.042
5.573
6.103
6.633
7.164
7.694
8.224
8.755
9.285
9.815
10.346
10.876
11.406
11.937
More

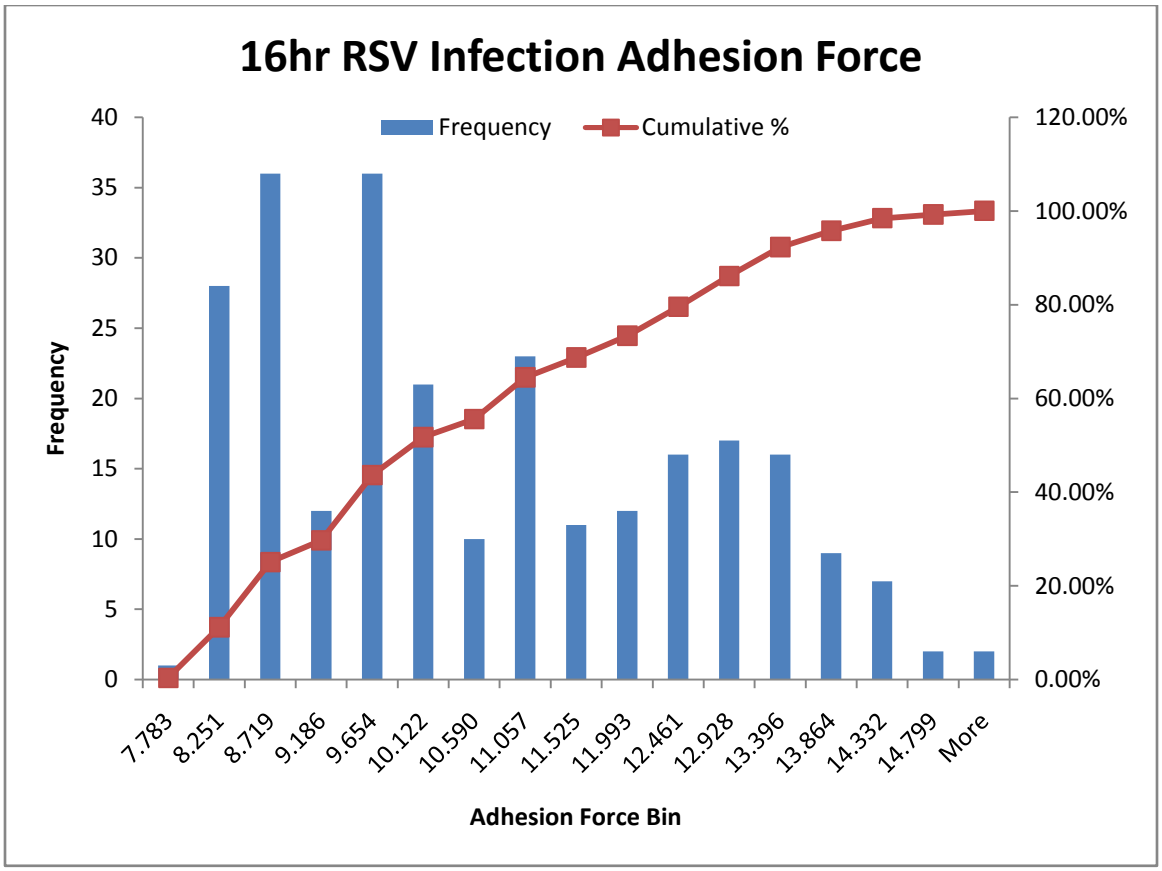
16hr RSV Infection Adhesion Force
Frequency
Cumulative %
Frequency
Adhesion Force Bin
0
5
10
15
20
25
30
35
40
0.00%
20.00%
40.00%
60.00%
80.00%
100.00%
120.00%
7.783
8.251
8.719
9.186
9.654
10.122
10.590
11.057
11.525
11.993
12.461
12.928
13.396
13.864
14.332
14.799
More

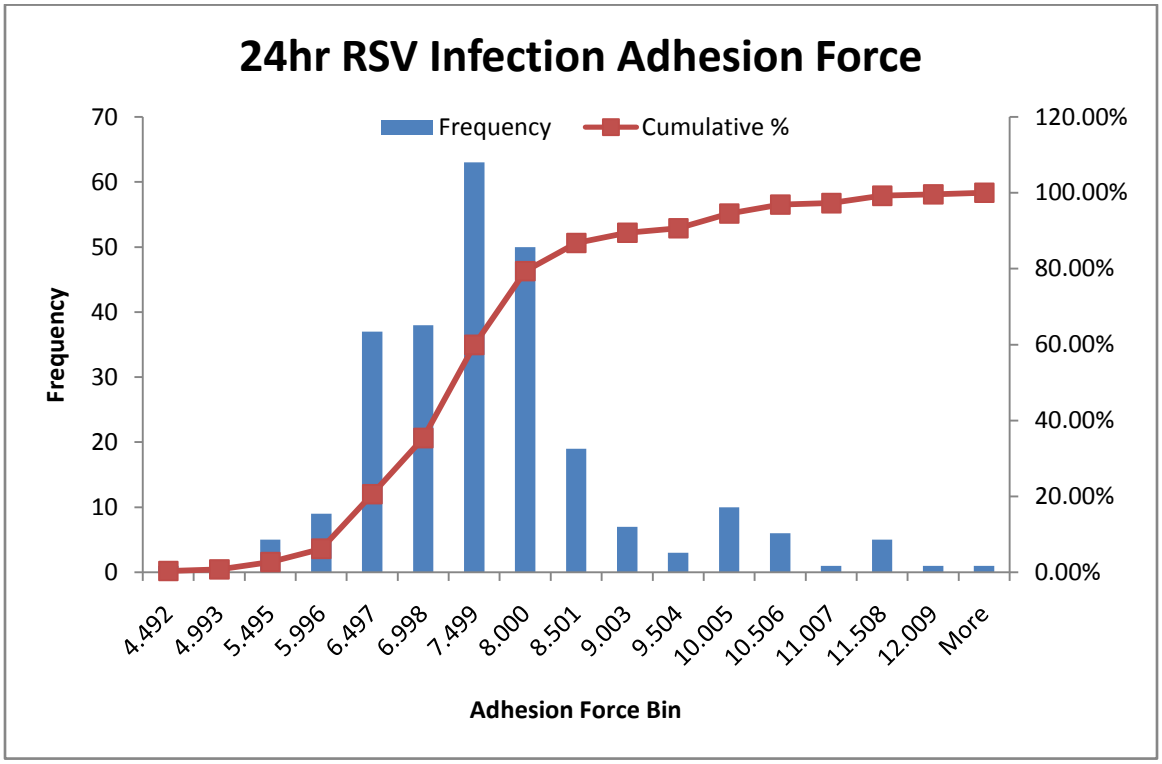
24hr RSV Infection Adhesion Force
Frequency
Cumulative %
Frequency
Adhesion Force Bin
0
10
20
30
40
50
60
70
0.00%
20.00%
40.00%
60.00%
80.00%
100.00%
120.00%
4.492
4.993
5.495
5.996
6.497
6.998
7.499
8.000
8.501
9.003
9.504
10.005
10.506
11.007
11.508
12.009
More

APPENDIX III

IMPORT TEXT FILES VBA ROUTINE

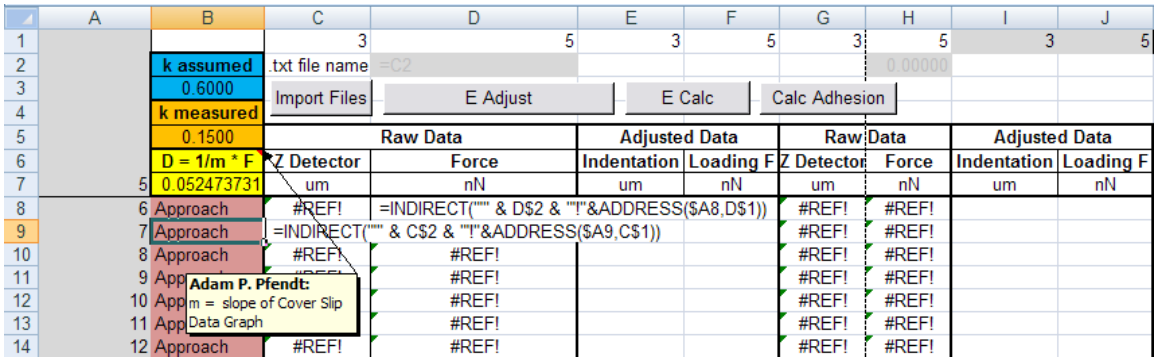

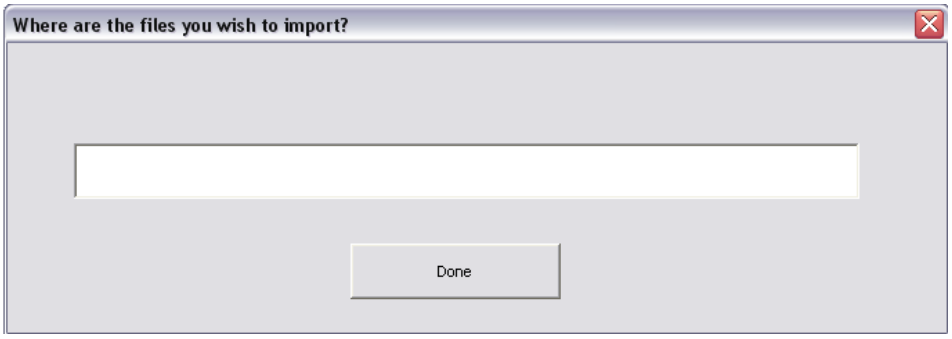


```
Private Sub OK_Click()
InputPath.Hide

Dim MyPath As String
Dim FilesInPath As String
Dim MyFiles() As String
Dim Fnum As Long
Dim mysheet As Worksheet
Dim basebook As Workbook

'turn off automatic calculation
Application.Calculation = xlManual

'Fill in the path\folder where the files are
MyPath = DestTBox.Value

'Add a slash at the end if the user forget it
If Right(MyPath, 1) <> "\" Then
MyPath = MyPath & "\"
End If

'If there are no txt files in the folder exit the sub
FilesInPath = Dir(MyPath & "*.txt")
```

```
If FilesInPath = "" Then
MsgBox "No files found"
Exit Sub
End If

On Error GoTo CleanUp
Application.ScreenUpdating = False
Set basebook = ThisWorkbook

'Fill the array(myFiles)with the list of txt files in the folder
Fnum = 0
Do While FilesInPath <> ""
Fnum = Fnum + 1
ReDim Preserve MyFiles(1 To Fnum)
MyFiles(Fnum) = FilesInPath
FilesInPath = Dir()
Loop

'Loop through all files in the array(myFiles)
If Fnum > 0 Then
For Fnum = LBound(MyFiles) To UBound(MyFiles)
Set mysheet = Worksheets.Add
mysheet.Name = MyFiles(Fnum)

' Imports Data from Files
With ActiveSheet.QueryTables.Add(Connection:="TEXT;" & MyPath & MyFiles(Fnum),
Destination:=Range("A1"))
    .Name = MyFiles(Fnum)
    .FieldNames = True
    .RowNumbers = False
    .FillAdjacentFormulas = False
    .PreserveFormatting = True
    .RefreshOnFileOpen = False
    .RefreshStyle = xlInsertDeleteCells
    .SavePassword = False
    .SaveData = True
    .AdjustColumnWidth = True
    .RefreshPeriod = 0
    .TextFilePromptOnRefresh = False
    .TextFilePlatform = 932
    .TextFileStartRow = 1
    .TextFileParseType = xlDelimited
    .TextFileTextQualifier = xlTextQualifierDoubleQuote
    .TextFileConsecutiveDelimiter = False
    .TextFileTabDelimiter = True
    .TextFileSemicolonDelimiter = False
    .TextFileCommaDelimiter = False
    .TextFileSpaceDelimiter = False
    .TextFileColumnDataTypes = Array(1)
    .TextFileTrailingMinusNumbers = True
    .Refresh BackgroundQuery:=False
  End With

'Enters name of sheet into _Data Summary sheet
Worksheets("_Data Summary").Range("C2:AUL2").Cells(1 + 4 * (Fnum - 1)).Value = MyFiles(Fnum)
```

```
Next Fnum
End If
Call SortSheets

CleanUp:
Application.ScreenUpdating = True

'turn on automatic calculation
'Application.Calculation = xlAutomatic

End Sub
```

APPENDIX IV

ELASTIC MODULUS CALCULATIONS VBA ROUTINE

```
Sub Adjust_Data()

' Adjusts all coverslip data so that it may be graphed

Dim i, j, k, ColNum, RowNum, DataEnd As Integer
Dim SheetName As String
Dim DataAnswer As Long
Dim Data(1 To 550, 1 To 5) As Single
Dim Discont As Single

'checks to see if the data is cell data or cover slip data
 DataAnswer = MsgBox("Is this cellular data?  If it is cover slip data then select 'No'.", vbYesNoCancel,
"Select Data Type")

If DataAnswer = vbCancel Then Exit Sub

'stores the name of the active sheet
SheetName = ActiveSheet.Name

'checks data for 500 entries
For i = 1 To 500

   'checks to see that a series exists
   If Sheets(SheetName).Range("C2:AUL2").Cells(1 + 4 * (i - 1)).Value <> "" Then

   'reads all data in that series into an array but omits the first 5 points from consideration
   'because they tend to be problematic and are omitted later anyway
   For ColNum = 1 To 2
   For RowNum = 1 To 550
      Data(RowNum, ColNum) = Sheets(SheetName).Range("C8:AUL1031").Cells(RowNum + 5, ColNum
+ 4 * (i - 1)).Value
      'MsgBox ("value: " & Data(RowNum, ColNum))
   Next RowNum
   Next ColNum

'data adjustment and calculation
   'checks to make sure that data is approach data by decrease of Z Detector value
   'will always keep the first data point
      j = 0
      RowNum = 1

      For RowNum = 1 To 550 - 1
         If (Data(RowNum + 1, 1) < Data(RowNum - j, 1)) Then
            'keeps data point
               Data(RowNum + 1 - j, 1) = Data(RowNum + 1, 1)
               Data(RowNum + 1 - j, 2) = Data(RowNum + 1, 2)
         Else
            'Replaces the last data point in the approach set with a dummy value to signify the end
```

```
            Data(RowNum + 1 - j, 1) = 100000
            Data(RowNum + 1 - j, 2) = 100000

          'increases counter to omit the data point on the next go around
            j = j + 1
        End If

    Next RowNum

'a loop that deletes all data points after the last value is found
    RowNum = 1

    For RowNum = 1 To 550 - 1
        If Data(RowNum, 1) = 100000 Then
            Data(RowNum + 1, 1) = 100000
            Data(RowNum + 1, 2) = 0
            Data(RowNum, 1) = 0
            Data(RowNum, 2) = 0
        End If

    Next RowNum

  'calculates the slopes between all the data points
    j = 0
    RowNum = 1

    For RowNum = 1 To 550 - 1
        Data(RowNum, 3) = (Data(RowNum + 1, 2) - Data(RowNum, 2)) / (Data(RowNum + 1, 1) -
Data(RowNum, 1) + 0.000001)
        'MsgBox ("slope = " & Data(RowNum, 3))
    Next RowNum


  'omits the flat portions of the graph where sample is not in contact or tip is not moving between loading
and unloading
  'by removing all points with an average slope less than a nominal value from consideration.  also
smooths out the curve
  'since very erratic data areas are omitted
    j = 1
    RowNum = 1

    For RowNum = 1 To 550 - 2
        If (Data(RowNum, 3) + Data(RowNum + 1, 3) + Data(RowNum + 2, 3)) / 3 < -10 Then

          'keeps the data points
            Data(RowNum + 1 - j, 4) = Data(RowNum + 1, 1)
            Data(RowNum + 1 - j, 5) = Data(RowNum + 1, 2)
        Else
          'counter to overwrite skipped point
            j = j + 1
        End If
    Next RowNum

'deletes first 5 values and to improve graph
For RowNum = 1 To 545
  Data(RowNum, 4) = Data(RowNum + 5, 4)
```

```
   Data(RowNum, 5) = Data(RowNum + 5, 5)
Next RowNum


'adjusts the Z Detector Data to become Distance Traveled instead of Z piezo position
   'reads in initial value into another position so it is not overwritten
   'might need to change to an average of the first few points

   Data(1, 3) = Data(1, 4)
   RowNum = 1
      For RowNum = 1 To 550
      If Data(RowNum, 4) <> 0 Then
            If Data(RowNum, 4) - Data(1, 3) < 0 Then
               Data(RowNum, 4) = -(Data(RowNum, 4) - Data(1, 3))
            Else
               Data(RowNum, 4) = (Data(RowNum, 4) - Data(1, 3))
            End If
         Else
         'do nothing
         End If
      Next RowNum


'adjusts the Force Data to zero at Z distance of zero
   Data(1, 3) = Data(1, 5)
   RowNum = 1
      For RowNum = 1 To 550

         If Data(RowNum, 5) <> 0 Then
            Data(RowNum, 5) = (Data(RowNum, 5) - Data(1, 3))
         Else
         'do nothing
         End If
      Next RowNum


'Enters adjusted data into sheet for cell data
If DataAnswer = vbYes Then

   'reads in formulas for Loading Force into sheet
   RowNum = 1
   ColNum = 2

   For RowNum = 1 To 550
   If Data(RowNum, 5) <> 0 Then
      Sheets(SheetName).Range("C8:AUL1031").Cells(RowNum, 2 + ColNum + 4 * (i - 1)).Formula =
"=k_measure*" & _
         Data(RowNum, 4)
   Else
      'writes in first value
      If RowNum = 1 Then
         Sheets(SheetName).Range("C8:AUL1031").Cells(RowNum, 2 + ColNum + 4 * (i - 1)).Formula =
"=k_measure*" & _
         Data(RowNum, 4)
      End If
   End If
```

```
    Next RowNum

'adjusts the Z Detector Data to allow for cantilever deflection in the cell formulas
    RowNum = 1
    ColNum = 2

    For RowNum = 1 To 550
    If Data(RowNum, 4) <> 0 Then
        Sheets(SheetName).Range("C8:AUL1031").Cells(RowNum, 1 + ColNum + 4 * (i - 1)).Formula =
"=m_cant*" & "k_measure/k_assume*" & _
            Data(RowNum, 5) & "-" & Data(RowNum, 4)
    Else
        'writes in first value
        If RowNum = 1 Then
            Sheets(SheetName).Range("C8:AUL1031").Cells(RowNum, 1 + ColNum + 4 * (i - 1)).Formula =
"=m_cant*" & "k_measure/k_assume*" & _
            Data(RowNum, 5) & "-" & Data(RowNum, 4)
        Else
        'ends the search
            DataEnd = RowNum
            RowNum = 551
        End If
    End If
    Next RowNum


'deletes data with force greater than .12.  After this value most of the graphs become erratic
    For RowNum = 1 To DataEnd
        If  Sheets(SheetName).Range("C8:AUL1031").Cells(RowNum, 2 + ColNum + 4 * (i - 1)).Value >
0.12 Then
            Sheets(SheetName).Range("C8:AUL1031").Cells(RowNum, 2 + ColNum + 4 * (i - 1)).Value = ""
            Sheets(SheetName).Range("C8:AUL1031").Cells(RowNum, 1 + ColNum + 4 * (i - 1)).Value = ""
        End If
    Next RowNum

'searches for the beginning of the linear discontinuity in data using a nominal difference in
'indentations of 0.015 um.  Decrease this number to increase sensitivity.
    For RowNum = 1 To DataEnd
        If Sheets(SheetName).Range("C8:AUL1031").Cells(RowNum + 1, 1 + ColNum + 4 * (i - 1)).Value -
_
            Sheets(SheetName).Range("C8:AUL1031").Cells(RowNum, 1 + ColNum + 4 * (i - 1)).Value >
0.015 Then
            'stores discontinuity location and ends search
                Discont = Sheets(SheetName).Range("C8:AUL1031").Cells(RowNum, 1 + ColNum + 4 * (i -
1)).Value
        RowNum = DataEnd + 10
        End If
    Next RowNum


'removes points in linear discontinuity from consideration.  Only removes a total of 16 points.
'This limit prevents it from deleting too much good data in the end of the run.  Highlights deleted cells.
    k = 1
    For RowNum = 1 To DataEnd
    If k < 17 Then
```

```
      If Sheets(SheetName).Range("C8:AUL1031").Cells(RowNum + 1, 1 + ColNum + 4 * (i - 1)).Value -
Discont > 0.015 Then
         Sheets(SheetName).Range("C8:AUL1031").Cells(RowNum + 1, 1 + ColNum + 4 * (i - 1)).Value =
""
         Sheets(SheetName).Range("C8:AUL1031").Cells(RowNum + 1, 2 + ColNum + 4 * (i - 1)).Value =
""
         Sheets(SheetName).Range("C8:AUL1031").Cells(RowNum + 1, 1 + ColNum + 4 * (i -
1)).Interior.Color = 255
         Sheets(SheetName).Range("C8:AUL1031").Cells(RowNum + 1, 2 + ColNum + 4 * (i -
1)).Interior.Color = 255
         k = k + 1
      End If
   Else
      RowNum = DataEnd + 10
   End If
   Next RowNum


Else

  'puts force formulas adjusted by spring constant into sheet
   RowNum = 1
   ColNum = 2

   For RowNum = 1 To 550
   If Data(RowNum, 5) <> 0 Then
      Sheets(SheetName).Range("C8:AUL1031").Cells(RowNum, 2 + ColNum + 4 * (i - 1)).Formula =
"=k_measure/k_assume*" & _
         Data(RowNum, 5)
   Else
      'writes in first value
      If RowNum = 1 Then
         Sheets(SheetName).Range("C8:AUL1031").Cells(RowNum, 2 + ColNum + 4 * (i - 1)).Formula =
"=k_measure/k_assume*" & _
         Data(RowNum, 5)
      End If
   End If
   Next RowNum

'enters the deflection data into the sheet
   RowNum = 1
   ColNum = 2

   For RowNum = 1 To 550
   If Data(RowNum, 4) <> 0 Then
      Sheets(SheetName).Range("C8:AUL1031").Cells(RowNum, 1 + ColNum + 4 * (i - 1)).Formula = "="
& Data(RowNum, 4)
   Else
      'writes in first value
      If RowNum = 1 Then
         Sheets(SheetName).Range("C8:AUL1031").Cells(RowNum, 1 + ColNum + 4 * (i - 1)).Formula =
"=" & Data(RowNum, 4)
      End If
   End If
   Next RowNum
```

```
End If

'clears the array of data
Erase Data


Else
'ends searching sequence
   i = 10000

End If

Next i

End Sub
```

APPENDIX V

ELASTIC MODULUS GRAPHING VBA ROUTINE

```
Sub Graph_Data()
'graphs all cover slip data in one graph to aquire F/D equation

Dim i, j, k, SeriesNum, RowNum, DataNum As Integer
Dim DataSheet, GraphSheet, ESheet As String
Dim MaxIndent(1 To 550) As Single
Dim GraphType As Long
Dim RegRange As Range

'asks to plot every set together or separately
 GraphType = MsgBox("Calculate elastic modulus and graph?  'No' graphs all data as one set.", vbYesNoCancel, "Graph Type")
 If GraphType = vbCancel Then Exit Sub

'graphs data as one set and adds a trend line
If GraphType = vbNo Then

'stores the name of the active sheet
DataSheet = ActiveSheet.Name

'creates new sheet
Sheets.Add Before:=Sheets(1)
GraphSheet = ActiveSheet.Name

'resets counters
j = 0
k = 0

'plots data for 500 entries
For i = 1 To 500

   'checks to see that a series exists
   If Sheets(DataSheet).Range("C2:AUL2").Cells(1 + 4 * (i - 1)).Value <> "" Then

   'reads all Z data in that series into a new sheet so it can be graphed
   For RowNum = 1 To 550
      If Sheets(DataSheet).Range("C8:AUL1031").Cells(RowNum, 3 + 4 * (i - 1)).Value <> "" Then

         Sheets(GraphSheet).Range("A1:AUL1031").Cells(RowNum + k, 1).Value = _
            Sheets(DataSheet).Range("C8:AUL1031").Cells(RowNum, 3 + 4 * (i - 1)).Value
         j = j + 1
      End If
   Next RowNum

   'reads all F data in that series into a new sheet so it can be graphed
   For RowNum = 1 To 550
      If Sheets(DataSheet).Range("C8:AUL1031").Cells(RowNum, 4 + 4 * (i - 1)).Value <> "" Then
```

```
            Sheets(GraphSheet).Range("A1:AUL1031").Cells(RowNum + k, 2).Value = _
               Sheets(DataSheet).Range("C8:AUL1031").Cells(RowNum, 4 + 4 * (i - 1)).Value
         End If
      Next RowNum

      End If
k = k + j
j = 0

Next i

'graphs the data on the sheet
   ActiveSheet.Shapes.AddChart.Select

   ActiveChart.SetSourceData Source:=Range(Sheets(GraphSheet).Name & "!$A$1:$A$1")
   ActiveChart.ChartType = xlXYScatter
   ActiveChart.SetElement (msoElementChartTitleAboveChart)
   ActiveChart.SetElement (msoElementPrimaryCategoryAxisTitleAdjacentToAxis)
   ActiveChart.SetElement (msoElementPrimaryValueAxisTitleRotated)
   ActiveChart.ChartTitle.Text = "Force vs. Z Detector"
   ActiveChart.Axes(xlValue, xlPrimary).AxisTitle.Text = "Loading Force in nN"
   ActiveChart.Axes(xlCategory, xlPrimary).AxisTitle.Text = "Indentation in µm"
   ActiveChart.Legend.Select
   Selection.Delete
   ActiveChart.Parent.Left = 125
   ActiveChart.Parent.Width = 750
   ActiveChart.Parent.Top = 20
   ActiveChart.Parent.Height = 450

'reads in the values
   ActiveChart.SeriesCollection(1).XValues = "='" & GraphSheet & "'!" & _
         Sheets(GraphSheet).Range("$A$1:$B$10000").Columns(1).Address
   ActiveChart.SeriesCollection(1).Values = "='" & GraphSheet & "'!" & _
         Sheets(GraphSheet).Range("$A$1:$B$10000").Columns(2).Address

'creates the trendline
   ActiveChart.SeriesCollection(1).Trendlines.Add
   ActiveChart.SeriesCollection(1).Trendlines(1).Select
   Selection.Intercept = 0
   Selection.DisplayEquation = True
   Selection.DisplayRSquared = True

'graphs each data set separately
Else

'stores the name of the active sheet
DataSheet = ActiveSheet.Name

'creates new sheet
Sheets.Add Before:=Sheets(1)
GraphSheet = ActiveSheet.Name

'resets counters
j = 0
k = 0
SeriesNum = 0
```

```
'plots data for 500 entries
For i = 1 To 500

   'checks to see that a series exists
   If Sheets(DataSheet).Range("C2:AUL2").Cells(1 + 4 * (i - 1)).Value <> "" Then

   'enters the series name into the sheet
   Sheets(GraphSheet).Range("A1:AUL1031").Cells(7, 2 * i - 1).Value =
Sheets(DataSheet).Range("C2:AUL2").Cells(1 + 4 * (i - 1)).Value
   SeriesNum = SeriesNum + 1

   'reads all Z data in that series into a new sheet so it can be graphed
   DataNum = 1
   For RowNum = 1 To 120
      If Sheets(DataSheet).Range("C8:AUL1031").Cells(RowNum, 3 + 4 * (i - 1)).Value <> "" Then

         Sheets(GraphSheet).Range("A9:AUL1031").Cells(DataNum, 2 * i - 1).Value = _
            Sheets(DataSheet).Range("C8:AUL1031").Cells(RowNum, 3 + 4 * (i - 1)).Value
         DataNum = DataNum + 1
         j = j + 1
         MaxIndent(i) = Sheets(DataSheet).Range("C8:AUL1031").Cells(RowNum, 3 + 4 * (i - 1)).Value
      End If
   Next RowNum


   'reads all F data in that series into a new sheet so it can be graphed
   DataNum = 1
   For RowNum = 1 To 120
      If Sheets(DataSheet).Range("C8:AUL1031").Cells(RowNum, 4 + 4 * (i - 1)).Value <> "" Then

         Sheets(GraphSheet).Range("A9:AUL1031").Cells(DataNum, 2 * i).Value = _
            Sheets(DataSheet).Range("C8:AUL1031").Cells(RowNum, 4 + 4 * (i - 1)).Value
         DataNum = DataNum + 1
      End If
   Next RowNum
   DataNum = DataNum - 1

'inserts linear regression equations
Sheets(GraphSheet).Range("A1").Value = "Slope"
Sheets(GraphSheet).Range("A2").Value = "Std Err"
Sheets(GraphSheet).Range("A3").Value = "R^2"
Sheets(GraphSheet).Range("A4").Value = "F"
Sheets(GraphSheet).Range("A5").Value = "ss reg"

      Set RegRange = Union(Sheets(GraphSheet).Range("B1:AUL5").Cells(1, 2 * i - 1), _
         Sheets(GraphSheet).Range("B1:AUL5").Cells(2, 2 * i - 1), _
         Sheets(GraphSheet).Range("B1:AUL5").Cells(3, 2 * i - 1), _
         Sheets(GraphSheet).Range("B1:AUL5").Cells(4, 2 * i - 1), _
         Sheets(GraphSheet).Range("B1:AUL5").Cells(5, 2 * i - 1))


   'RegRange.FormulaArray = "=LINEST(R[8]C[0]:R[84]C[0],R[8]C[-1]:R[84]C[-1],0,TRUE)"
   RegRange.FormulaArray = "=LINEST(R[8]C[0]:R[" & DataNum + 7 & "]C[0],R[8]C[-1]:R[" & _
      DataNum + 7 & "]C[-1],0,TRUE)"
```

```
    End If
j = 0

Next i

'graphs the data on the sheet
    ActiveSheet.Shapes.AddChart.Select

    ActiveChart.SetSourceData Source:=Range(Sheets(GraphSheet).Name & "!$A$9:$A$9")
    ActiveChart.ChartType = xlXYScatter
    ActiveChart.SetElement (msoElementChartTitleAboveChart)
    ActiveChart.SetElement (msoElementPrimaryCategoryAxisTitleAdjacentToAxis)
    ActiveChart.SetElement (msoElementPrimaryValueAxisTitleRotated)
    ActiveChart.ChartTitle.Text = "Loading Force vs. Indentation"
    ActiveChart.Axes(xlValue, xlPrimary).AxisTitle.Text = "Loading Force in nN"
    ActiveChart.Axes(xlCategory, xlPrimary).AxisTitle.Text = "Indentation in µm"
    ActiveChart.Legend.Select
    Selection.Delete
    ActiveChart.Parent.Left = 125
    ActiveChart.Parent.Width = 750
    ActiveChart.Parent.Top = 20
    ActiveChart.Parent.Height = 450
    ActiveChart.SetElement (msoElementLegendRight)

'reads in the values into a different series for each data set on the graph
For i = 1 To SeriesNum
    ActiveChart.SeriesCollection(i).Name = Sheets(GraphSheet).Range("A7:AUL1031").Cells(1, 2 * i - 1)
    ActiveChart.SeriesCollection(i).XValues = "='" & GraphSheet & "'!" & _
            Sheets(GraphSheet).Range("$A$9:$B$10000").Columns(2 * i - 1).Address
    ActiveChart.SeriesCollection(i).Values = "='" & GraphSheet & "'!" & _
            Sheets(GraphSheet).Range("$A$9:$B$10000").Columns(2 * i).Address
        ActiveChart.SeriesCollection.NewSeries

Next i


'performs elastic modulus calculation on a new sheet
'stores the name of the active sheet
DataSheet = ActiveSheet.Name

'creates new sheet
Sheets.Add Before:=Sheets(1)
ESheet = ActiveSheet.Name

'inserts column titles and formatting
Sheets(ESheet).Range("A1").Value = "Name"
Sheets(ESheet).Range("B1").Value = "Reg. Slope"
Sheets(ESheet).Range("C1").Value = "R^2"
Sheets(ESheet).Range("D1").Value = "Indent. (um)"
Sheets(ESheet).Range("E1").Value = "E Mod."
    Range("A1:E1").Select
    Selection.Font.Bold = True
    With Selection
        .HorizontalAlignment = xlCenter
```

```
        .VerticalAlignment = xlBottom
        .WrapText = False
        .Orientation = 0
        .AddIndent = False
        .IndentLevel = 0
        .ShrinkToFit = False
        .ReadingOrder = xlContext
        .MergeCells = False
    End With
    Columns("A:A").ColumnWidth = 21.29
    Columns("B:B").EntireColumn.AutoFit
    Columns("D:D").EntireColumn.AutoFit
    Columns("D:D").EntireColumn.AutoFit

'imports name, slope, R2, and maximum indentation
For i = 1 To SeriesNum
'name
Sheets(ESheet).Range("A2:A100").Cells(i, 1).Value = Sheets(DataSheet).Range("A7:ZZ7").Cells(1, 2 * i -
1).Value
'slope
Sheets(ESheet).Range("B2:B100").Cells(i, 1).Value = Sheets(DataSheet).Range("B1:ZZ1").Cells(1, 2 * i -
1).Value
'R2
Sheets(ESheet).Range("C2:C100").Cells(i, 1).Value = Sheets(DataSheet).Range("B3:ZZ3").Cells(1, 2 * i -
1).Value
'maximum indentation
Sheets(ESheet).Range("D2:D100").Cells(i, 1).Value = MaxIndent(i)
'Elastic Modulus
Sheets(ESheet).Range("E2:E100").Cells(i, 1).Value = Sheets(ESheet).Range("B2:B100").Cells(i, 1).Value
/ _
    MaxIndent(i) * 0.328587

Next i

Erase MaxIndent

End If

End Sub
```

APPENDIX VI

ADHESION FORCE CALCULATION VBA ROUTINE

```
Sub Adhesion()
' Adjusts all coverslip data so that it may be graphed

Dim i, j, k, ColNum, RowNum, DataEnd, SeriesNum As Integer
Dim SheetName, AdhSheet As String
Dim Data(1 To 550, 1 To 5) As Single
Dim AdhesionForce(1 To 100) As Single

'stores the name of the active sheet
SheetName = ActiveSheet.Name

'checks data for 500 entries
For i = 1 To 500

   'checks to see that a series exists
   If Sheets(SheetName).Range("C2:AUL2").Cells(1 + 4 * (i - 1)).Value <> "" Then

   'reads all data in that series into an array but omits the first 5 points from consideration
   'because they tend to be problematic and are omitted later anyway
   For ColNum = 1 To 2
   For RowNum = 1 To 550
      Data(RowNum, ColNum) = Sheets(SheetName).Range("C8:AUL1031").Cells(RowNum + 500,
ColNum + 4 * (i - 1)).Value
   Next RowNum
   Next ColNum

'data adjustment and calculation
   'checks to make sure that data is retraction data by increase of Z Detector value
   'will always keep the first data point
      j = 0
      RowNum = 1

      For RowNum = 1 To 550 - 1
         If (Data(RowNum + 1, 1) > Data(RowNum - j, 1)) Then
            'keeps data point
               Data(RowNum + 1 - j, 1) = Data(RowNum + 1, 1)
               Data(RowNum + 1 - j, 2) = Data(RowNum + 1, 2)
         Else
            'Replaces the last data point in the approach set with a dummy value to signify the end
               Data(RowNum + 1 - j, 1) = 100000
               Data(RowNum + 1 - j, 2) = 100000

            'increases counter to omit the data point on the next go around
               j = j + 1
         End If
      Next RowNum

'a loop that deletes all data points after the last value is found
```

```
        RowNum = 1

        For RowNum = 1 To 550 - 1
            If Data(RowNum, 1) = 100000 Then
                Data(RowNum + 1, 1) = 100000
                Data(RowNum + 1, 2) = 0
                Data(RowNum, 1) = 0
                Data(RowNum, 2) = 0
            End If
        Next RowNum
'deletes dummy value
Data(RowNum, 1) = 0

'enters retraction data into the sheet
  'puts force data into sheet
    RowNum = 1
    ColNum = 2

    For RowNum = 1 To 550
    If Data(RowNum, 2) <> 0 Then
        Sheets(SheetName).Range("C8:AUL1031").Cells(RowNum, 2 + ColNum + 4 * (i - 1)).Formula =
"=k_measure/k_assume*" & _
            Data(RowNum, 2)
    Else
        'writes in first value
        If RowNum = 1 Then
            Sheets(SheetName).Range("C8:AUL1031").Cells(RowNum, 2 + ColNum + 4 * (i - 1)).Formula =
"=k_measure/k_assume*" & _
            Data(RowNum, 2)
        End If
    End If
    Next RowNum

'enters the deflection data into the sheet
    RowNum = 1
    ColNum = 2

    For RowNum = 1 To 550
    If Data(RowNum, 1) <> 0 Then
        Sheets(SheetName).Range("C8:AUL1031").Cells(RowNum, 1 + ColNum + 4 * (i - 1)).Formula = "="
& Data(RowNum, 1)
    Else
        'writes in first value
        If RowNum = 1 Then
            Sheets(SheetName).Range("C8:AUL1031").Cells(RowNum, 1 + ColNum + 4 * (i - 1)).Formula =
"=" & Data(RowNum, 1)
        End If
    End If
    Next RowNum

'searches data for biggest jump between three data points for adhesion force value.
For RowNum = 1 To 550
    If Sheets(SheetName).Range("C8:AUL1031").Cells(RowNum + 2, 2 + ColNum + 4 * (i - 1)).Value - _
        Sheets(SheetName).Range("C8:AUL1031").Cells(RowNum, 2 + ColNum + 4 * (i - 1)).Value >
AdhesionForce(i) Then
```

```
      AdhesionForce(i) = Sheets(SheetName).Range("C8:AUL1031").Cells(RowNum + 2, 2 + ColNum + 4
* (i - 1)).Value - _
      Sheets(SheetName).Range("C8:AUL1031").Cells(RowNum, 2 + ColNum + 4 * (i - 1)).Value
   End If
Next RowNum


Else
'ends searching sequence
   SeriesNum = i - 1
   i = 10000
End If


Next i

'inserts a new sheet and enters all adhesion data onto it
'creates new sheet
Sheets.Add Before:=Sheets(1)
AdhSheet = ActiveSheet.Name

For i = 1 To SeriesNum
'Data set name
Sheets(AdhSheet).Range("A2:A100").Cells(i,  1).Value  =  Sheets(SheetName).Range("C2:AUL2").Cells(1
+ 4 * (i - 1)).Value
'Adhesion force
Sheets(AdhSheet).Range("B2:B100").Cells(i, 1).Value = AdhesionForce(i)
Next i

'formats sheet
Sheets(AdhSheet).Range("A1").Cells.Value = "Data Set"
Sheets(AdhSheet).Range("B1").Cells.Value = "Adhesion Force (kPa)"
Columns("A:A").EntireColumn.AutoFit
Columns("B:B").EntireColumn.AutoFit
End Sub
```

VITA

Adam Palmer Pfendt was born on October 30, 1985 in Cincinnati, OH. He graduated from Boone County High School in Florence, KY in 2004 and was accepted into the University of Louisville Speed School of Engineering that fall as a Grawemeyer Scholar and National Merit Honorable Mention.

He held four different offices in the Speed School Student Council board of directors including President and Vice President where he coordinated the Engineering-Expo for two straight years. Now an alumnus of Triangle Fraternity, he held multiple chair positions including Community Service Chair, Social Chair, Fryberger Chair, and Flag Football Coach. Adam was also a member of Tau Beta Pi, the American Institute of Chemical Engineers, Omicron Delta Kappa, and the Order of Omega.

Adam received his Bachelors of Science in Chemical Engineering in the spring of 2008 with highest honors and was awarded the D.A. Richards Award. He completed his Masters of Engineering in Chemical Engineering in the summer of 2009 with highest honors and received the W.S. Speed Award for service to the Speed School of Engineering.